Table 1
Details and efficacy of corticosteroid therapy.

Pt no	*PCDH19* mutation	Age at onset (m)	Age at CS TX	CS	Route & dose	Target symptom	Simultaneous TX	Usual duration of Sz cluster	Result	Present intellect
1	p.L719*	13	2y4m	mPSL	IV, 30 mg/kg, 3d	Sz cluster	MDL CBZ CZP VPA LTG LEV	Days ~2 wk	Disappeared after 1st IV	Normal 5y1m
			2y10m	mPSL	IV, 30 mg/kg, 3d	Sz cluster			Disappeared after 1st IV Recurred in 2 wk w/fever[a]	
			2y11m	mPSL	IV, 30 mg/kg, 3d	Sz cluster			Disappeared after 1st IV Recurred in 1wk w/fever	
			3y0m	mPSL	IV, 10 mg/kg, 3d	Sz cluster			Disappeared after 1st IV	
			3y4m	BET	Oral, 0.01 mg/kg, 3d When fever appeared	Sz prevention			No or mild recurrence	
			4y1m	PSL	Oral, 1–1.5 mg/kg, 3d When fever appeared	Sz prevention			No or mild recurrence	
2	p.K120Rfs*3	10	10m	mPSL	IV, 30 mg/kg, 3d	Sz cluster	MDL PB ACV IVIG EDV	–	Disappeared after 1st IV Recurred in 1wk	Moderate delay 3y
3	p.D417H p.D596Y	5	1y11m	mPSL	IV, 20 mg/kg, 2d	Sz cluster	MDL fPHT CLB LEV KBr DZP	Days ~2wk	Disappeared after 1st IV	Normal 2y8m
			2y1m	mPSL	IV, 20 mg/kg, 3d	Sz cluster			Disappeared after 1st IV	
			2y2m	mPSL	IV, 20 mg/kg, 2d	Sz cluster			Disappeared after 1st IV	
			2y5m	mPSL	IV, 10 mg/kg, 1d *fol. by* 20 mg/kg, 1d	Sz cluster			Disappeared after 2nd IV	
			2y7m	mPSL	IV, 20 mg/kg, 1d	Sz cluster			Disappeared after 1st IV Recurred in 9d w/flu	
			2y7m	mPSL	IV, 20 mg/kg, 2d	Sz cluster			Disappeared after 1st IV	
4	p.D596G	6	1y0m	mPSL	IV, 30 mg/kg, 3d	Encephalopatic symptoms	CBZ fPHT LDC PB	1d	Disappeared after 1st IV	Hyperactive 1y6m
5	p.D45Gfs*43	8	11y5m	PSL	IV, 0.35 mg/kg x1 *fol. by* Oral, 1 mg/kg[b]	Sz cluster	KBr CZP	Half a day	Disappeared after 1st IV	Moderate delay 11y8m
			11y6m	PSL	IV, 0.35 mg/kg x1 *fol. by* Oral, 1 mg/kg	Sz cluster			Disappeared after 1st IV Recurred in 1wk w/fever	
			11y6m	PSL	IV, 0.35 mg/kg x1 *fol. by* Oral, 1 mg/kg	Sz cluster			Disappeared after 1st IV	
			11y8m	PSL	IV, 0.35 mg/kg x2 *fol. by* Oral, 1 mg/kg	Sz cluster			Disappeared after 2nd IV	

[a] Noted when seizures recurred within 3 weeks after corticosteroid administration.
[b] In Patient 5, oral prednisolone was gradually tapered off. Pt no, Patient number; m, month(s); CS, corticosteroid; TX, treatment; Sz, seizure; y, year(s); mPSL, methylprednisolone; BET, betamethasone; PSL, prednisolone; IV, intravenous route; d, day(s); MDL, midazolam; CBZ, carbamazepine; CZP, clonazepam; VPA, valproic acid; LTG, lamotrigine; LEV, levetiracetam; wk, week(s); PB, phenobarbital; ACV, acyclovir; IVIG, intravenous immunoglobulin; EDV, edaravone; *fol. by*, followed by; fPHT, fosphenytoin; CLB, clobazam; KBr, potassium bromide; DZP, diazepam; LDC, lidocaine.

3.2. *ab-NR and further anti-neuronal autoantibody assays*

Eight of the nine patients who underwent the assay showed positivity to multiple epitopes in the serum or CSF (Patients 1–7 and 9, 88.9%, Table 2). The epitopes included GluN1-NT, which has been reported to be critical for the emergence of neuropsychiatric symptoms in anti-NMDA-receptor encephalitis [6]. Patients 1 and 2 had high CSF titers of antibodies during the acute phase (>10 SD). Patient 6 showed positivity in the CSF at onset and in serum half a year later. Patients 3, 5, and 9 underwent follow-up assays, and their titers were found to decrease over time. In Patient 5, immunohistochemical analysis during seizure recurrence at age 11, using serum drawn before prednisolone administration, revealed autoantibodies to the cytoplasm of hippocampal neurons, as demonstrated in hippocampal slices taken from rats (Supplementary Fig. b). The assay failed to identify the epitope. These results suggest that following seizure clusters, an immune reaction occurs non-specifically to degraded neuronal proteins, including NMDA-type glutamate receptor, inside and subsequently outside the brain. Such reactions appear to be strong at early ages, but do not show a uniform pattern.

4. Discussion

This study revealed the therapeutic potency of corticosteroids for acute symptoms in *PCDH19*-FE. The rapid and efficient response was remarkable and might be a useful indicator for this disease. The cases of Patients 1 and 9 suggested that oral corticosteroids taken during interictal periods might exert some prophylactic effects, but further assessments are necessary to establish this.

Table 2
Results of assay for antibodies to *N*-methyl-D-aspartate-type glutamate receptor.

Pt no	*PCDH19* mutation	Age at onset (m)	Age at assay	Serum					Cerebrospinal fluid				
				GluN2B		GluN1	GluD2		GluN2B		GluN1	GluD2	
				NT	CT	NT	NT	CT	NT	CT	NT	NT	CT
1	p.L719*	13	2y5m	1.61	**3.12**		1.93	0.45	**14.10**	**15.10**		**10.80**	**8.10**
2	p.K120Rfs*3	10	11m						**15.42**				
			4y2m	**2.21**	1.53	**3.58**	**3.63**						
3	p.D417H	5	11m	**2.17**	**2.94**	**3.62**	**2.85**						
	p.D596Y		1y0m						**3.39**	**3.28**	**2.81**	**2.35**	
	Heterozygous		1y7m	**2.65**	**2.21**	**2.17**	1.95						
			1y10m	1.23	0.37	0.72	0.99						
4	p.D596G	6	1y0m						**2.67**	**2.39**	1.51	1.68	
5	p.D45Gfs*43	8	9m	+					–	+			
			3y5m	–					–				
6	Whole del	10	11m	0.57	1.70		0.46	(0.34)	1.61	**2.73**		1.34	0.75
			1y5m	**2.33**	**2.73**		**2.48**	0.92	0.46	1.18		1.13	0.70
7	p.Asn340Ser	9	8y1m	**3.49**	**2.07**	**9.55**	1.87						
8	p.R198L	7	6y5m	1.70	0.90	1.78	1.68						
9	p.Y366Lfs*10	5	6y0m	**9.52**		**12.50**	**9.20**		−0.88		−1.37	−1.08	
			8y5m	0.60	(0.35)	0.25	0.37						

Results are expressed as standard deviation (SD, enzyme-linked immunosorbent assay) or plus/minus sign (immunoblot, Patient 5 only). Bold values denote positivity (≥2 SD or +). Blanks are unexamined. *Patients who received corticosteroid treatments. Pt no, Patient number; m, month(s); NT, N-terminal; CT, C-terminal; y, year(s); Whole del, Whole *PCDH19* deletion.

Despite such efficacy, short-term administration of corticosteroids provided only transient effects and had no potential for preventing further seizure clusters. Therefore, the clinical benefit will be limited for cases with frequent recurrences such as Patients 3 and 5. Moreover, excessive amounts of corticosteroids may have adverse effects, actually increasing seizure-proneness as described below. These findings suggest that the attending physician should consider discontinuing corticosteroid administration for acute treatment soon after seizure disappearance. Indication for treatment should be based on various patient conditions such as age, seizure severity, and comorbid infections.

Corticosteroids may exert primarily excitatory/pro-convulsive actions on brain neurons both *in vitro* and *in vivo*, especially under chronic stress conditions such as epilepsy [9]. Despite this, the therapeutic efficacy of corticosteroids is well established in many intractable epilepsies such as West syndrome, Landau-Kleffner syndrome, and autoimmune epilepsy/encephalitis [10]. In these diseases, clinical improvements after corticosteroid administration are usually delayed and are probably mediated by mechanisms such as immunosuppression and feedback inhibition of corticotropin-releasing hormone secretion. In our patients, however, the clinical effects appeared quickly, usually immediately after the initial administration. Moreover, significant brain inflammation was not found, suggesting a particular pathogenesis and mechanism of action of corticosteroids in *PCDH19*-FE.

Such a mechanism may be restoration of blood-brain barrier (BBB) integrity [11]. This is known to be a crucial action of corticosteroids, the underlying molecular basis of which has been partially elucidated [12]. Seizures are easily triggered by a mild breakdown of brain homeostasis due to a compromised BBB, which can be prevented or alleviated by corticosteroid administration [13]. Although PCDH19 is abundantly expressed in brain neurons, it is unclear how the heterozygous mutation in *PCDH19* leads to epilepsy in females. "Cellular interference," that is, the presence of somatic mosaicism in PCDH19 expression between normal and abnormal neurons, is the currently proposed explanation for such sex-specific pathogenesis, but the concept is very theoretical and has yet to be established. However, *PCDH19* is also expressed in the BBB. In mouse, the BBB-specific transcriptome included *PCDH19*, and *PCDH19* expression in microvascular endothelial cells was significantly higher in the brain than in the liver or lung [14]. Although currently no human evidence exists, this study suggests that PCDH19 plays a role in the BBB, and speculatively, that *PCDH19* mutation leads to a functional BBB vulnerability, that underlies the pathogenesis of *PCDH19*-FE.

Interestingly, *PCDH19* expression may be significantly altered in the BBB during systemic inflammation, which is the predisposing factor for seizure recurrence in *PCDH19*-FE. In cultured mouse brain microvascular endothelial cells, treatment with lupus serum or an activated complement, C5a, significantly down-regulated miR-320a expression [15]. *PCDH19* is one potential target of this microRNA. Although systemic inflammation will impair BBB function to some extent [16], the impairment may be exacerbated in patients with *PCDH19*-FE, probably due to PCDH19 insufficiency. The resulting seizure clusters will further exacerbate the BBB dysfunction by inducing brain inflammation. Corticosteroids may ameliorate such dysfunction and thus the acute neurological symptoms.

Other aspects of *PCDH19*-FE and the findings of this study are also consistent with the BBB hypothesis: The seizures mainly involve the limbic system, which is anatomically close to some of the periventricular regions that lack a BBB due to their endocrine roles; seizure occurrence and remission are strongly age-related, and BBB integrity also develops age-dependently; abs-NR in our patients covered multiple epitopes of various subunits, and Patient 8 had antibodies to some neuronal cytoplasmic component(s) as well. These results indicate that anti-neuronal antibodies may be produced in *PCDH19*-FE non-specifically and commonly. Various neuronal proteins will be degraded by recurrent seizures and the compromised BBB may then facilitate leakage of such degraded proteins into the bloodstream. This may induce non-specific sensitization to them outside the brain, resulting in the high rate of anti-neuronal autoantibody positivity seen in our patients. Thus, the abs-NR found in our patients does not represent an autoimmune pathogenesis.

However, a possible modifying effect of the abs-NR on the neurological phenotype in our patients with *PCDH19*-FE can also be considered. The seroprevalence of abs-NR has been found to be identical between patients with psychiatric diseases, including schizophrenia, and healthy individuals, but the disease phenotypes were more severe in patients with compromised BBBs than in those without [17]. Serum abs-NR could have passed the compromised BBB and worsened the psychiatric symptoms of these patients. In anti-NMDA-receptor encephalitis, a primary involvement of antibodies to GluN1-NT in causing its neuropsychiatric symptoms has been suggested [6]. Therefore if BBB compromise exists in *PCDH19*-FE, the anti-GluN1-NT could be partially responsible for the neuropsychiatric symptoms also seen in this disease.

This study proposes corticosteroid treatment as an efficacious adjunctive treatment for the acute symptoms of *PCDH19*-FE and suggests BBB involvement in this disease. Although *PCDH19*-FE is rare, future multicenter clinical trials should be conducted to verify the acute and long-term efficacy of corticosteroid treatment and to define the therapeutic indications of such treatment, since the present study is only a retrospective review of 5 patients. In addition, reliable animal models should be devised to elucidate the entire molecular pathogenesis of *PCDH19*-FE. Importantly, not only must neurons be studied, but also other actors such as the BBB and the inflammatory system as well.

Conflict of interest

All authors wish to confirm that there are no known conflict of interest associated with this publication.

Acknowledgments

The authors are indebted to all members of the study family for their helpful cooperation. This work was supported by Grants-in-Aid for Scientific Research (A) (24249060) to SH, (C) (21591342, 23591238 and 24591537) to YT, and (C) (26461552) to NH, a Grant-in-aid for Challenging Exploratory Research (25670481) to SH, Bilateral Joint Research Projects to SH, and a Grant-in-aid for Young Scientists (B) (24791095) to NH from the Japan Society for the Promotion of Science (JSPS); by Grants for Scientific Research on Innovative Areas (221S0002 and 25129708) to SH from the Ministry of Education, Culture, Sports, Science and Technology (MEXT); by a MEXT-supported Program for the Strategic Research Foundation at Private Universities 2013–2017 to SH; by a Grant-in-aid for the Research on Measures for Intractable Diseases (No. H26-Nanji-Ippan-49 and 51) to SH, and Comprehensive Research on Disability Health and Welfare and Research on Rare and Intractable Diseases to YT from the Ministry of Health, Labor and Welfare (MHLW); by an Intramural Research Grant (24-7) for Neurological and Psychiatric Disorders of NCNP to SH; by the Joint Usage/Research Program of Medical Research Institute, Tokyo Medical and Dental University to SH; by research grants from The Mitsubishi Foundation to SH, from Takeda Scientific Foundation to SH, from Kiyokun Foundation to SH, from The Japan Epilepsy Research Foundation to YT, and from Kaibara Morikazu Medical Science Promotion Foundation to NH.

Appendix A. Supplementary data

Supplementary data associated with this article can be found, in the online version, at http://dx.doi.org/10.1016/j.seizure.2015.02.006.

References

[1] Dibbens LM, Tarpey PS, Hynes K, Bayly MA, Scheffer IE, Smith R, et al. X-linked protocadherin 19 mutations cause female-limited epilepsy and cognitive impairment. Nat Genet 2008;40:776–81.
[2] Kim SY, Yasuda S, Tanaka H, Yamagata K, Kim H. Non-clustered protocadherin. Cell Adh Migr 2011;5:97–105.
[3] Higurashi N, Shi X, Yasumoto S, Oguni H, Sakauchi M, Itomi K, et al. PCDH19 mutation in Japanese females with epilepsy. Epilepsy Res 2012;99:28–37.
[4] Marini C, Darra F, Specchio N, Mei D, Terracciano A, Parmeggiani L, et al. Focal seizures with affective symptoms are a major feature of PCDH19 gene-related epilepsy. Epilepsia 2012;53:2111–9.
[5] Higurashi N, Nakamura M, Sugai M, Ohfu M, Sakauchi M, Sugawara Y, et al. PCDH19-related female-limited epilepsy: further details regarding early clinical features and therapeutic efficacy. Epilepsy Res 2013;106:191–9.
[6] Dalmau J, Gleichman AJ, Hughes EG, Rossi JE, Peng X, Lai M, et al. Anti-NMDA-receptor encephalitis: case series and analysis of the effects of antibodies. Lancet Neurol 2008;7:1091–8.
[7] Ekizoglu E, Tuzun E, Woodhall M, Lang B, Jacobson L, Icoz S, et al. Investigation of neuronal autoantibodies in two different focal epilepsy syndromes. Epilepsia 2014;55:414–22.
[8] Fujita K, Yuasa T, Takahashi Y, Tanaka K, Sako W, Koizumi H, et al. Antibodies to *N*-methyl-D-aspartate glutamate receptors in Creutzfeldt-Jakob disease patients. J Neuroimmunol 2012;251:90–3.
[9] Castro OW, Santos VR, Pun RY, McKlveen JM, Batie M, Holland KD, et al. Impact of corticosterone treatment on spontaneous seizure frequency and epileptiform activity in mice with chronic epilepsy. PLoS One 2012;7:e46044.
[10] Gupta R, Appleton R. Corticosteroids in the management of the paediatric epilepsies. Arch Dis Child 2005;90:379–84.
[11] Forster C, Waschke J, Burek M, Leers J, Drenckhahn D. Glucocorticoid effects on mouse microvascular endothelial barrier permeability are brain specific. J Physiol 2006;573:413–25.
[12] Salvador E, Shityakov S, Forster C. Glucocorticoids and endothelial cell barrier function. Cell Tissue Res 2014;355:597–605.
[13] Marchi N, Granata T, Freri E, Ciusani E, Ragona F, Puvenna V, et al. Efficacy of anti-inflammatory therapy in a model of acute seizures and in a population of pediatric drug resistant epileptics. PLoS One 2011;6:e18200.
[14] Daneman R, Zhou L, Agalliu D, Cahoy JD, Kaushal A, Barres BA. The mouse blood-brain barrier transcriptome: a new resource for understanding the development and function of brain endothelial cells. PLoS One 2010;5:e13741.
[15] Eadon MT, Jacob A, Cunningham PN, Quigg RJ, Garcia JG, Alexander JJ. Transcriptional profiling reveals that C5a alters microRNA in brain endothelial cells. Immunology 2014;143:363–73.
[16] Marchi N, Fan Q, Ghosh C, Fazio V, Bertolini F, Betto G, et al. Antagonism of peripheral inflammation reduces the severity of status epilepticus. Neurobiol Dis 2009;33:171–81.
[17] Hammer C, Stepniak B, Schneider A, Papiol S, Tantra M, Begemann M, et al. Neuropsychiatric disease relevance of circulating anti-NMDA receptor autoantibodies depends on blood-brain barrier integrity. Mol Psychiatry 2014;19:1143–9.

RESEARCH ARTICLE

AMERICAN JOURNAL OF medical genetics PART A

Mutations in *PIGL* in a Patient with Mabry Syndrome

Ikuma Fujiwara,[1] Yoshiko Murakami,[2] Tetsuya Niihori,[3] Junko Kanno,[1] Akiko Hakoda,[1] Osamu Sakamoto,[1] Nobuhiko Okamoto,[4] Ryo Funayama,[5] Takeshi Nagashima,[5] Keiko Nakayama,[5] Taroh Kinoshita,[2] Shigeo Kure,[1] Yoichi Matsubara,[3,6] and Yoko Aoki[3]*

[1]Department of Pediatrics, Tohoku University School of Medicine, Sendai, Japan

[2]WPI Immunology Frontier Research Center and Research Institute for Microbial Diseases, Osaka University, Osaka, Japan

[3]Department of Medical Genetics, Tohoku University School of Medicine, Sendai, Japan

[4]Department of Medical Genetics, Osaka Medical Center and Research Institute for Maternal and Child Health, Izumi, Japan

[5]Division of Cell Proliferation, United Centers for Advanced Research and Translational Medicine, Tohoku University Graduate School of Medicine, Sendai, Japan

[6]National Research Institute for Child Health and Development, Tokyo, Japan

Manuscript Received: 10 June 2014; Manuscript Accepted: 8 December 2014

Mabry syndrome, hyperphosphatasia mental retardation syndrome (HPMRS), is an autosomal recessive disease characterized by increased serum levels of alkaline phosphatase (ALP), severe developmental delay, intellectual disability, and seizures. Recent studies have revealed mutations in *PIGV, PIGW, PIGO, PGAP2,* and *PGAP3* (genes that encode molecules of the glycosylphosphatidylinositol (GPI)-anchor biosynthesis pathway) in patients with HPMRS. We performed whole-exome sequencing of a patient with severe intellectual disability, distinctive facial appearance, fragile nails, and persistent increased serum levels of ALP. The result revealed a compound heterozygote with a 13-bp deletion in exon 1 (c.36_48del) and a two-base deletion in exon 2 (c.254_255del) in phosphatidylinositol glycan anchor, class L (*PIGL*) that caused frameshifts resulting in premature terminations. The 13-bp deletion was inherited from the father, and the two-base deletion was inherited from the mother. Expressing c.36_48del or c.254_255del cDNA with an HA-tag at the C- or N-terminus in *PIGL*-deficient CHO cells only partially restored the surface expression of GPI-anchored proteins (GPI-APs). Nonsynonymous changes or frameshift mutations in *PIGL* have been identified in patients with CHIME syndrome, a rare autosomal recessive disorder characterized by colobomas, congenital heart defects, early onset migratory ichthyosiform dermatosis, intellectual disability, and ear abnormalities. Our patient did not have colobomas, congenital heart defects, or early onset migratory ichthyosiform dermatosis and hence was diagnosed with HPMRS, and not CHIME syndrome. These results suggest that frameshift mutations that result in premature termination in *PIGL* cause a phenotype that is consistent with HPMRS.

Key words: glycosylphosphatidylinositol anchor; Mabry syndrome; hyperphosphatasia mental retardation syndrome; genetic testing

How to Cite this Article:
Fujiwara I, Murakami Y, Niihori T, Kanno J, Hakoda A, Sakamoto O, Okamoto N, Funayama R, Nagashima T, Nakayama K, Kinoshita T, Kure S, Matsubara Y, Aoki Y. 2015. Mutations in *PIGL* in a patient with mabry syndrome. Am J Med Genet Part A 167A:777–785.

INTRODUCTION

In 1970, Mabry et al. reported three siblings with increased serum levels of alkaline phosphatase (ALP), severe developmental delay, intellectual disability, and seizures [Mabry et al., 1970]. Subsequently, a condition displaying the aforementioned symptoms was referred to as hyperphosphatasia with mental retardation (HPMR) syndrome or Mabry syndrome [Krawitz et al., 2010]. Other clinical features included distinctive facial features such as hypertelorism, a

Conflict of interest: none.
Grant sponsor: Biomedical Research Core of Tohoku University Graduate School of Medicine; Grant sponsor: Ministry of Health, Labor and Welfare of Japan; Grant sponsor: Japan Society for the Promotion of Science; Grant numbers: C: 25461535, C: 23590363; Grant sponsor: Takeda Science Foundation; Grant sponsor: Ministry of Education, Culture, Sports, Science, and Technology of Japan; Grant number: 25129705.
*Correspondence to:
Yoko Aoki, M.D., Ph.D, Department of Medical Genetics, Tohoku University School of Medicine, 1-1 Seiryo-machi, Sendai 980-8574, Japan. E-mail: aokiy@med.tohoku.ac.jp
Article first published online in Wiley Online Library (wileyonlinelibrary.com): 23 February 2015
DOI 10.1002/ajmg.a.36987

broad nasal bridge, long palpebral fissures, and a tented mouth, as well as some degree of brachytelephalangy [Horn et al., 2011]. Variable neurological abnormalities, including seizures and muscular hypotonia, were also associated with this condition. Extensive biochemical analysis showed that hyperphosphatasia was unlikely to be the result of increased activity of osteoblastic cells or hepatobiliary dysfunction, and the causes of HPMRS were unknown [Kruse et al., 1988].

In 2010, Krawitz et al. performed whole-exome sequencing of three siblings with HPMRS (OMIM 239300) and identified homozygous or compound heterozygous mutations in *PIGV* in a total of six families with HPMRS [Krawitz et al., 2010]. *PIGV* encodes a molecule that acts as the second mannosyltransferase in the glycosylphosphatidylinositol (GPI) anchor biosynthesis pathway. Subsequently, mutations in *PIGO, PGAP2, PGAP3*, and *PIGW*, which are also involved in GPI biosynthesis, have been identified in individuals with HPMRS (OMIM 614749, OMIM 614207, OMIM 615716, and OMIM 610275, respectively) [Krawitz et al., 2012, 2013; Hansen et al., 2013; Chiyonobu et al., 2014; Howard et al., 2014]. In this study, we performed whole-exome sequencing of a family with HPMRS but without mutations in *PIGV* and *PIGO* and identified compound heterozygous mutations in *PIGL*.

MATERIAL AND METHODS

Exome Sequencing

DNA was extracted using a standard protocol from blood samples of an affected female and her parents. Control DNA was obtained from 192 healthy Japanese individuals. This study was approved by the Ethics Committee of Tohoku University School of Medicine. We obtained informed consent and specific consent for photographs from the parents of the affected individual.

Exome sequencing was conducted on an individual with HPMRS. Targeted enrichment was performed using the SureSelect Human All Exon V2 kit. Exon-enriched DNA libraries were sequenced on the Illumina Hiseq 2000 for 101 bp. Burrows-Wheeler Aligner (BWA) was used to align the sequence reads to the human genome (hg19); all parameters of BWA were kept at the default settings. Following removal of duplicates from the alignments, realignment around known indels, recalibration, and SNP/indel calling were performed with Genome Analysis Toolkit (GATK, 1.5) [McKenna et al., 2010]. ANNOVAR was used for the annotation against the RefSeq database and dbSNP [Wang et al., 2010].

Sanger Sequencing

Each exon with flanking intronic sequences in *PIGV, PIGO, PIGN, PIGB*, and *PIGL* was amplified with primers based on GenBank sequences (NM_017837.2, NM_152850.3, NM_176787.4, NM_004855.4, and NM_004278.3, respectively). The M13 reverse or forward sequence was added to the 5′ end of the polymerase chain reaction (PCR) primers for use as sequencing primers. PCR was performed in 15 μl of solution containing 67 mM Tris–HCl (pH 8.8), 6.7 mM $MgCl_2$, 17 mM NH_4SO_4, 6.7 μM EDTA, 10 mM β-ME, 1.5 mM dNTPs, 10% (v/v) DMSO, 1 μM of each primer, 25 ng genomic DNA and 1 U of Taq DNA polymerase. The reaction consisted of 37 cycles of denaturation at 94°C for 20 sec, annealing at the indicated temperature for 30 sec and extension at 72°C for 30 sec. PCR products were purified using MultiScreen PCR plates (Millipore, Billerica, MA). The purified products were sequenced on an ABI 3500xL Genetic Analyzer (Applied Biosystems, Foster City, CA).

For subcloning, PCR products of exon 1 and 2 in *PIGL* were subcloned using a pTOPO TA cloning kit (Invitrogen, Carlsbad, CA) and transformed in TOP10F competent cells (Invitrogen). Plasmids were purified from each colony and sequenced.

Flow Cytometry

Surface expression of GPI-anchored proteins (GPI-APs) of granulocytes was determined by staining cells with PE-conjugated mouse anti-human CD59 (H19), anti-human DAF (IA10), anti-human CD24 (ML5), anti-human CD16 (3G8) antibodies, each isotype IgG (BD Biosciences, Franklin Lakes, NJ) and Alexa 488-conjugated inactivated aerolysin (FLAER; Protox Biotech, Canada). CD59, DAF, CD24, and CD16 are GPI-APs and FLAER binds to surface GPI-APs. The surface expression was then analyzed using a flow cytometer (Canto II; BD Biosciences) and FlowJo software (Tommy Digital, Inc., Tokyo, Japan).

Functional Analysis

PIGL-deficient CHO cells (M2S2) [Nakamura et al., 1997] were transiently transfected with *PIGL* cDNA that was driven by the strong SRα promoter (pME hPIGL-HA or pME HA-hPIGL). Two days later, cells were stained with anti-CD59, anti-DAF and FLAER and analyzed by flow cytometry. Lysates were separated using SDS–PAGE and Western blotting was performed.

RESULTS

Clinical Report

The patient was the first child of healthy and non-consanguineous Japanese parents. She was born at 33 weeks and 3 days of gestation by caesarean because of maternal infection. Her weight and height at birth were 2,510 g and 51 cm, respectively. She was treated with oxygen inhalation for several days because of transient tachypnea. She was suspected as having Beckwith–Wiedemann syndrome because of hypotonia, a large tongue, separation of the rectus abdominis muscle, and coarse facial features.

At 4 months of age, the patient's serum levels of ALP were found to be extremely high at 4,394 IU/L (Normal, 395–1,289 IU/L) and she was referred to our hospital. A radiograph of her hands showed a slight delay of bone maturation and slight dilation of the ulnar metaphysis. Alpha D3 administration was started at 5 months and ended at 1 year and 8 months of age. Laboratory investigations for inborn errors of metabolism, including toluidine blue staining in a urine sample, glycosaminoglycan in the urine, and lysosome enzymes, were normal. Karyotyping analysis on cultured leukocytes and subtelomere MLPA, FISH for 17p11.2 detecting Smith–Magenis syndrome, and array CGH analysis were all normal.

Twitching of the extremities with epileptic discharge on EEG started at 4 months of age and required anti-convulsant therapy. Brain CT and MRI showed dilatation of the bilateral lateral ven-

tricles, third and fourth ventricles and sub-arachnoid space, as well as hypoplasia of the cerebellar vermis. She was suspected as having mild deafness (right: 30 dB and left 45 dB).

At 1 year and 10 months, her weight and height were 7.9 kg (−2 SD) and 80 cm (−1 SD), respectively. Her craniofacial features included midface hypoplasia, hypertelorism, long palpebral fissures, strabismus, depressed nasal bridge, anteverted nostrils, tented upper lip vermilion, full cheeks, a high palate, and ear anomalies (Fig. 1A). Teeth eruption was not observed. In the extremities, the 2nd and 3rd digits were overlapping. The terminal phalanges of the hands and feet were short with hypoplastic nails. Her development was as follows: head control at 5 months, crawling at 1 year and 7 months, sitting at 2 year and 3 months, and walking while holding onto something at 2 years and 7 months. At 3 years and 6 months, she was unable to walk independently, and speech development was markedly delayed. ALP remained persistently elevated (3,000–4,500 U/L, Fig. 1B).

Molecular and Biochemical Analysis

Mutation screening for genes in GPI biosynthesis showed that no mutations were identifiable by Sanger sequencing analysis in any exons coding for *PIGV, PIGO, PIGN,* and *PIGB.* We then performed exome sequencing with a sample from the proband. Using the sequencing analysis pipeline from BWA and GATK, we identified approximately 8,883 nonsynonymous, nonsense, splicing site variations, coding insertions, and/or deletions (indels) per individual. Filtering steps using variant databases (dbSNP132, the 1,000 Genome Project database and ESP 5,400) resulted in the identification of 216 variants. Two frameshift mutations in *PIGL* (c.36_48del [p.Leu13Alafs*11] and c.254_255del [p.Glu86Aspfs*2]) were detected as variants in genes that participate in the GPI-anchor biosynthesis (hsa00563) and the GPI-anchor biosynthesis (hsa00563)/metabolic pathway (hsa00110) in KEGG pathway, respectively. Sanger sequencing validated the heterozygous state of the two variants in *PIGL* (Fig. 2A). Two variants resulted in a premature termination and it was assumed that truncated proteins were produced (Fig. 2B).

Subcloning of PCR products of exons 1 and 2 from parental samples followed by sequencing showed that the father was heterozygous for c.36_48del and the mother was heterozygous for c.254_255del in *PIGL*, thus confirming the compound heterozygosity in the affected individual (Fig. 2A).

The c.36_48del and c.254_255del in *PIGL* were not reported in dbSNP132, the 1,000 Genome Project database or in ESP 5,400. c.254_255del, and not c.36_48del, was reported in one in 1,000 Japanese exomes (http://www.genome.med.kyoto-u.ac.jp /SnpDB/) and identified in 1 in 192 of our in-house Japanese controls in a hetrozygous manner, suggesting that c.254_255del could be identified at a frequency of 1:200–1:1000 in Japanese people.

These genomic analyses suggested that the patient has *PIGL*-deficiency, which is one of the inherited GPI deficiencies. More than 100 mammalian proteins are modified by a GPI anchor at their C terminus [Krawitz et al., 2010]. The expression of GPI-APs have been decreased in other inherited GPI deficiencies [Maydan et al., 2011; Chiyonobu et al., 2014; Howard et al., 2014]. To examine if the GPI-APs decreased in cells from our patient, peripheral blood cells were analyzed by flow cytometry. Surface expression of various GPI-APs on the granulocytes from the patient (Fig. 3, thick lines) was severely decreased (2% of the control in CD16 expression) compared with that from the normal samples (dotted lines).

PIGL-deficient CHO cells (M2S2) [Nakamura et al., 1997] were transiently transfected with wild type (Fig. 4, dotted line),

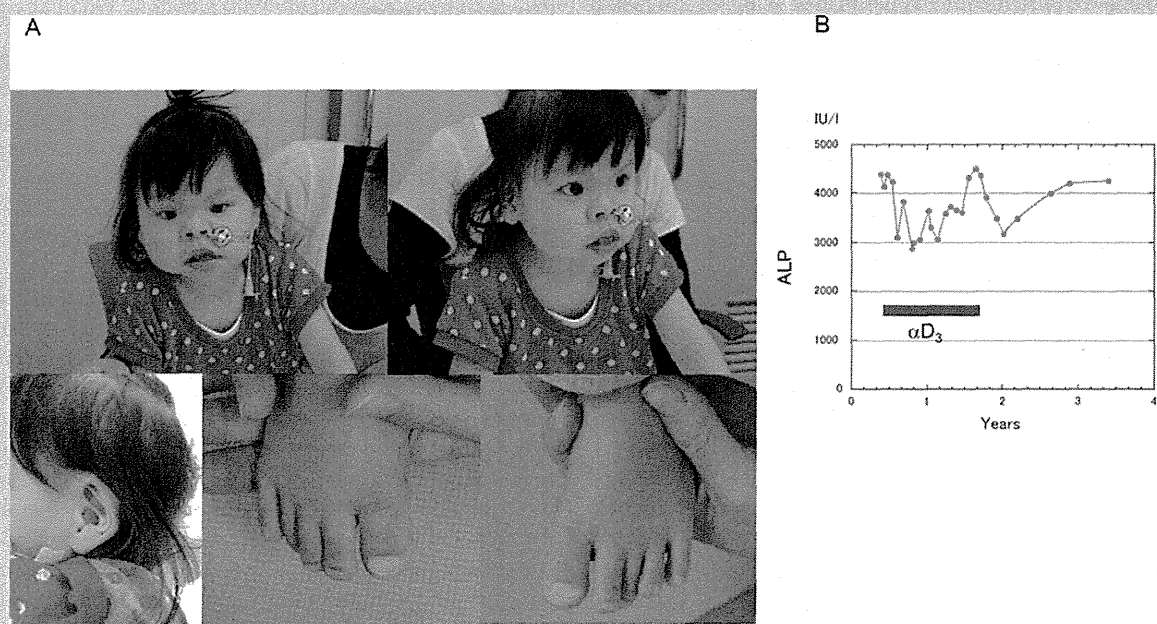

FIG. 1. Clinical manifestation of the proband. A: Photos of the girl at 2 years and 7 months of age. B: Serum levels of ALP in the patient.

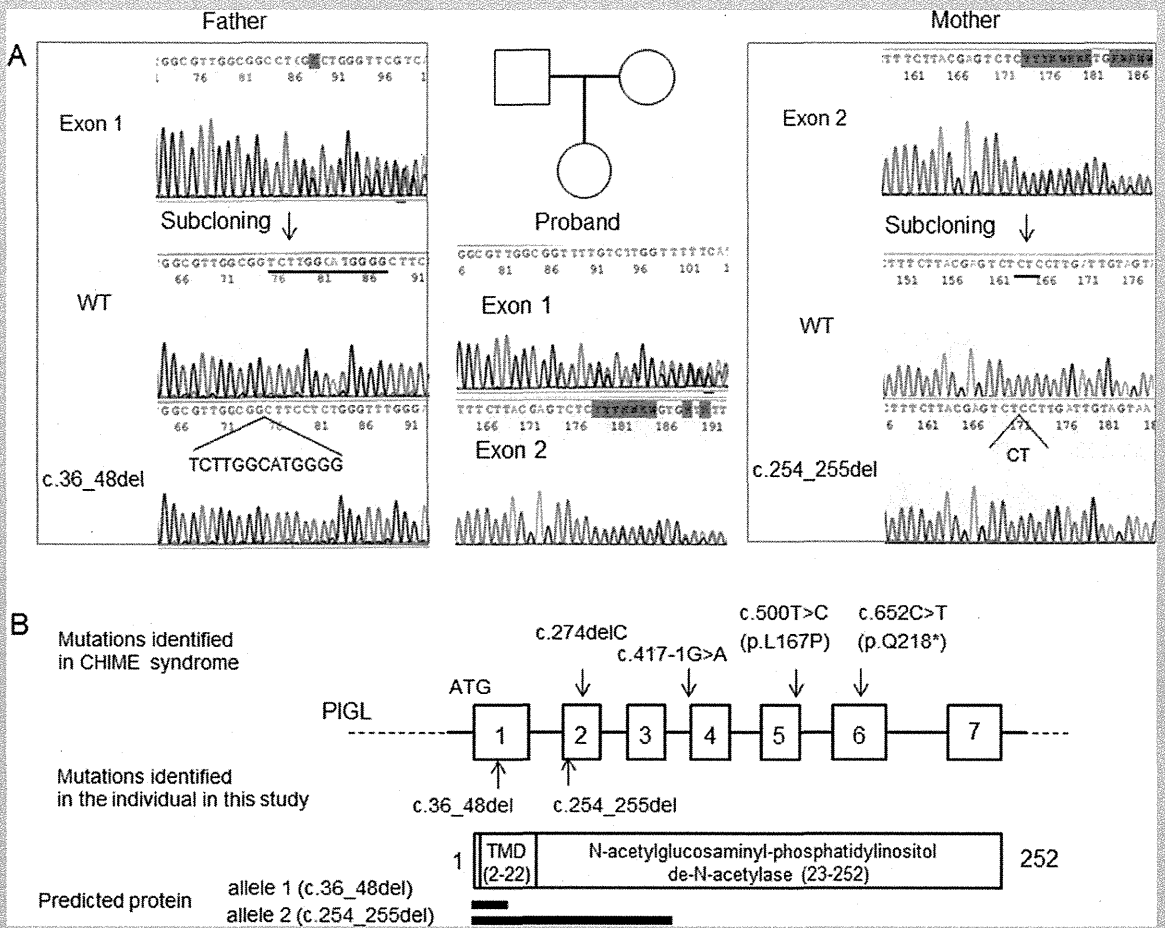

FIG. 2. Sanger sequencing of the family. A: Mutation analysis of the individual and her parents. B: The genomic structure of *PIGL* and mutations identified in CHIME syndrome and this study.

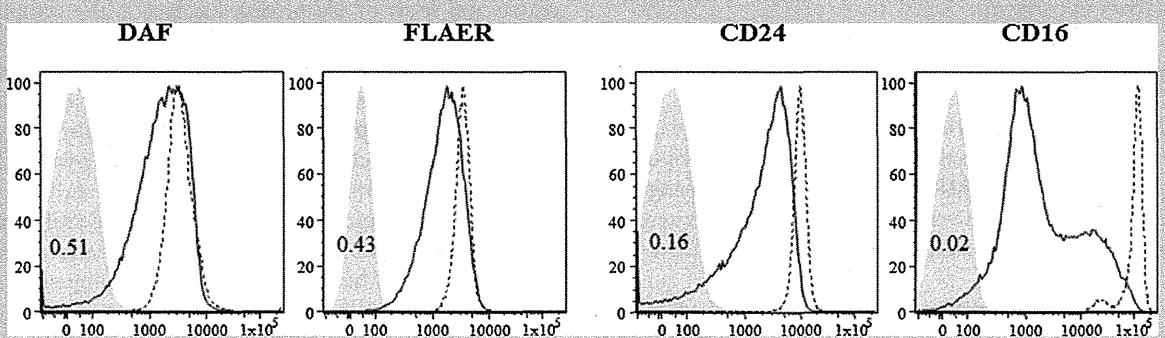

FIG. 3. Flow cytometry of granulocytes. Surface expression of various GPI-APs on the granulocytes from the patient (thick lines) was severely decreased compared with that from the normal samples (dotted lines). Light shadows are isotype controls. The value of the mean fluorescent intensity of each sample against normal is shown in each panel.

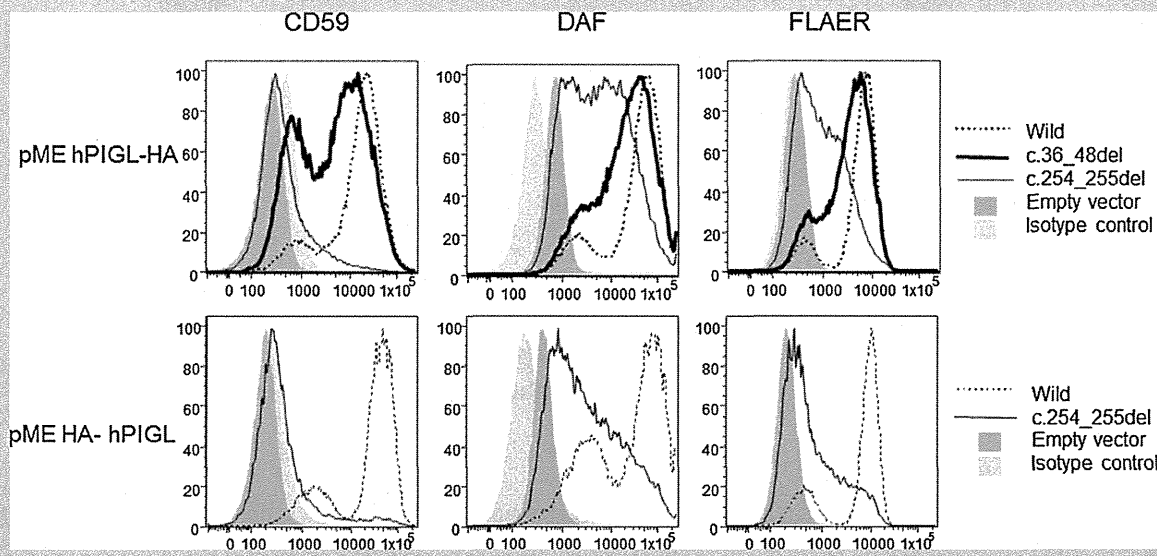

FIG. 4. PIGL-deficient CHO cells (M2S2) [Nakamura et al., 1997] were transiently transfected with wild type (dotted line), the c.36_48del mutant (thick line), or the c.254_255del mutant (thin line) PIGL cDNA that was driven by the strong SRα promoter (pME hPIGL-HA or pME HA-hPIGL) with an HA-tag at the C-(upper panels) or N-terminus (lower panels). Two days later, cells were stained with anti-CD59, anti-DAF and FLAER and analyzed by flow cytometry. The gray shadow denotes empty vector transfections; light gray shadows are isotype controls.

c.36_48del mutant (thick line) or c.254_255del mutant (thin line) *PIGL* cDNA with an HA-tag at the C-terminus (upper panels) or at the N-terminus (lower panels). Both mutants could only partially restore the surface expression of GPI-APs. The activity of the c.254_255del mutant was severely affected, and the N-terminal tagged construct had almost no activity. These results suggested that the remaining activity was not due to the truncated proteins. Faint bands (* and **) could be detected in the lysate of C-terminally tagged c.36_48 mutant transfected cells (Fig. 5A), which corresponded to the isoforms starting at the downstream methionines (2 and 3 of Fig. 5B) that showed residual PIGL activity. No band could be detected from the lysate of the c.256_255 mutant tagged at either terminus (data not shown).

DISCUSSION

We report on the case of a girl with distinctive facial features, severe intellectual disability, and persistent increased serum levels of ALP who was diagnosed with HPMRS. Whole-exome sequencing identified two frameshift mutations in *PIGL*, which were inherited from the father and mother, suggesting that *PIGL* mutations are responsible for HPMRS.

Many eukaryotic cell surface proteins are bound to the cell membrane by a GPI-anchor. More than 20 different gene products are involved in GPI biosynthesis [Fujita and Kinoshita 2012]. Recent studies revealed that genetic defects in various components of the GPI-anchor biosynthesis pathway cause inherited GPI deficiencies. Somatic mutations in *PIGA* in hematopoietic stem cells cause paroxysmal nocturnal hemoglobinuria [Ware et al., 1994]. A promoter mutation in *PIGM* causes portal venous thrombosis and absence seizures [Almeida et al., 2006]. Germline mutations in *PIGN* and *PIGA* cause congenital anomalies with hypotonia and seizures [Maydan et al., 2011; Johnston et al., 2012]. Germline mutations in *PIGV*, *PIGO*, *PGAP2*, *PGAP3*, and *PIGW* have been identified in individuals with HPMRS [Krawitz et al., 2010, 2012, 2013; Chiyonobu et al., 2014; Howard et al., 2014]. Recently, mutations in *PIGT* have been identified in a family with intellectual disability [Kvarnung et al., 2013]. Thus, the clinical spectrum of disorders caused by the GPI-anchor deficiency has expanded.

PIGL encodes a 252 amino acid endoplasmic reticulum (ER) protein, located on the ER membrane with one transmembrane region and most of the protein located on the cytoplasmic side [Nakamura et al., 1997]. PIGL is involved in the second step of GPI biosynthesis, which is de-N-acetylation of N-acetylglucosaminyl-phosphatidylinositol (GlcNAc-PI). Following de-N-acetylation, glucosaminyl-phosphatidylinositol (GlcN-PI) flips to the luminal side of ER where GlcN-PI undergoes further extensions followed by its transfer to acceptor proteins [Nakamura et al., 1997; Watanabe et al., 1999]. Mutations in *PIGL* have been identified in CHIME syndrome, an autosomal recessive disorder characterized by colobomas, congenital heart defects, early onset migratory ichthyosiform dermatosis, intellectual disability, and ear anomalies, including conductive hearing loss [Ng et al., 2012]. Our patient manifested severe intellectual disability, seizures, ear anomalies, and feeding difficulties, which overlapped with symptoms of CHIME syndrome [Ng et al., 2012]. However, our patient did not have colobomas, congenital heart defects, early onset migratory ichthyosiform, or genitourinary abnormalities. Inherited GPI

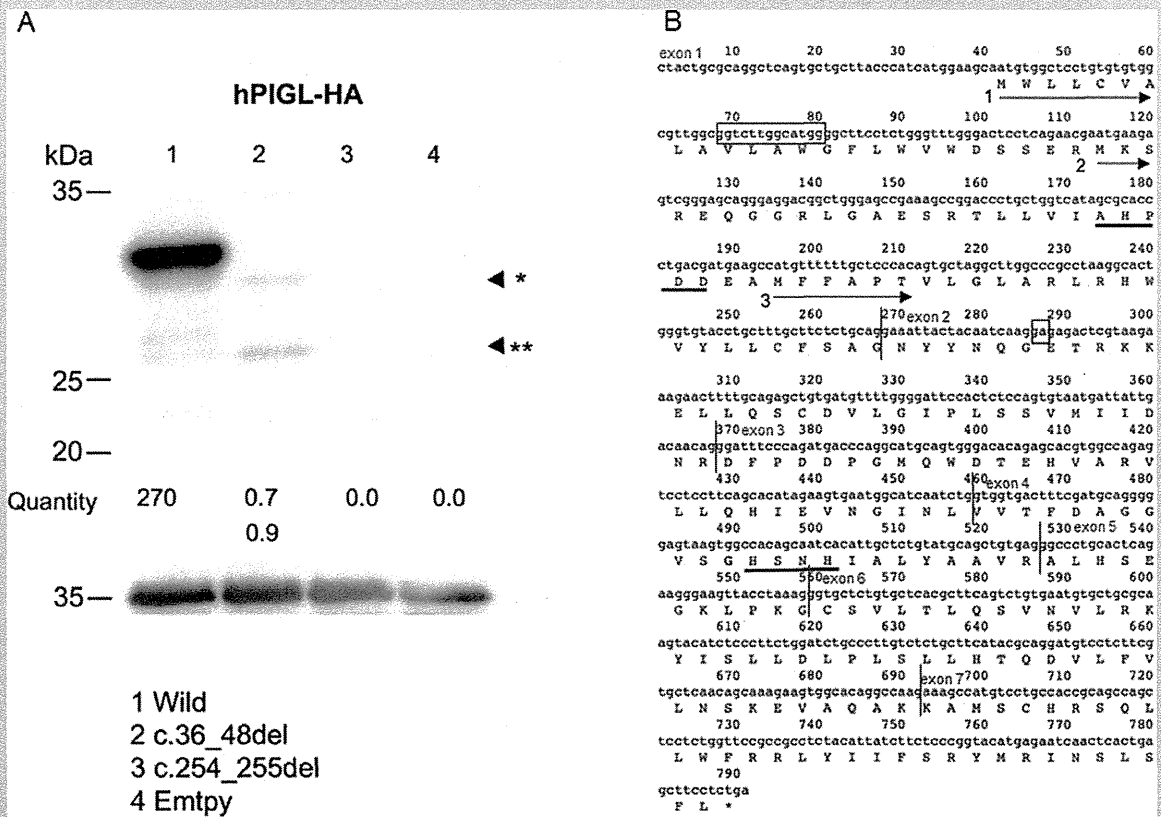

FIG. 5. Functional analysis. A: Lysates were separated by SDS–PAGE and western blotting was performed. Faint bands (* and **) could be detected from the lysate of the C-terminally tagged c.36_48 mutant transfected cells, which corresponded to the isoform starting from the down stream methionines (2 and 3 in Fig. 5B) that showed residual *PIGL* activity. No band could be detected from the lysate of the c.256_255 mutant tagged at either terminus. (Normalized with the intensities of GAPDH, the loading control, and luciferase activities used for evaluating transfection efficiencies). B: The sequence of *PIGL* cDNA; thick lines, conserved motifs; numbered arrows, three translation initiation sites; boxes, deletions in this patient.

deficiencies caused by a defect in the GPI-biosynthesis genes should show similar symptoms that result from the decreased expression of various GPI-APs on the cell surface. The severity depends on the amount of the GPI-anchor produced in ER, and the individual's genetic background may also have some influence on variations. Clinical manifestations in our patient were more similar to those in individuals with HPMRS, including hypertelorism, long palpebral fissures, broad nasal tip, tented upper lip, brachytelephalangy, severe intellectual disability and persistent hyperphosphatasia (Table I) [Horn et al., 2011]. These results suggest that frameshift mutations in 5′ terminus of *PIGL* cause HPMRS. It is possible that *PIGL* mutations identified in patients with CHIME syndrome might have higher residual activities.

Brain CT and MRI of our patient showed cerebellar atrophy. Frontotemporal atrophy and cerebellar hypoplasia have been shown in patients with *PIGT* mutations [Kvarnung et al., 2013]. Cerebral and cerebellar atrophy have been reported in a patient with *PIGO* mutation [Nakamura et al., 2014] and in patients with *PIGN* mutations [Maydan et al., 2011; Ohba et al., 2014], suggesting that cerebral atrophy and cerebellar atrophy are common features in patients with inherited GPI deficiencies. It is of note that cerebral atrophy has been also observed in patients with CHIME syndrome [Shashi et al., 1995; Schnur et al., 1997].

Our previous study demonstrated that mutant CHO cells having defects in the later step genes efficiently secrete ALP into the medium, whereas most ALP produced in the early step mutants is degraded in the cells [Murakami et al., 2012] because GPI transamidase is activated through binding with a mannose-containing GPI intermediate before this enzyme complex processes the precursor proteins for release. However, there are cases that are inconsistent with these experimental results. Some *PIGA*-deficient patients showed mild elevation of ALP (412 IU/L, normal range, 39–117 IU/L) [Johnston et al., 2012]. Elevation of ALP has not been reported in previously reported patients with *PIGL* deficiencies [Ng et al., 2012]. There may be differences in in vitro culture and in vivo body conditions; however, the primary reason for these differences needs to be identified in the future.

TABLE I. Summary of Clinical Features in Our Patient and HPMRS Patients With *PIGV*, *PIGO*, *PGAP2*, *PGAP3*, and *PIGW* Mutations

	Our study (PIGL)	PIGV	PIGO	PGAP2	PGAP3	PIGW
References		Horn et al. [2011]; Krawitz et al. [2010, 2012]	Krawitz et al. [2012]	Krawitz et al. [2013]; Hansen et al. [2013]	Howard et al. [2014]	Chiyonobu et al. [2014]
Sex	1 female	9 females and 5 males	3 females	4 female and 1 male	4 females and 2 males	1 proband
Age at assessment	1 year 10 months	7 months–17 years	20 months–15 years	3.5 and 28 years	2–17 years	ND
Origin	Japanese	German, Moroccan, Dutch, Polish, British, and European American	European	Finnish, Turkish, Northwestern Syria and Pakistani	Pakistani, American and Saudi–Arabian	Japanese
Height	−1.0 SD	normal in 13/14	−1.4 to −4.2 SD	−0.9 to 0.6 SD	normal in 4/5	ND
Weight	−2.0 SD	normal in 13/14	+0.6 to −3.3 SD	−1.0 SD to normal	normal in 4/5	ND
OFC	−1.0 SD	normal in 12/14	+0.7 to −5.5 SD	−4.5 SD to normal	−3.0 SD to normal	ND
Hyperphosphatasia	+	14/14	3/3	4/4	5/5	+
Intellectual disability	severe	14/14	3/3	4/4	5/5	+
Age at walking	delayed	delayed	delayed	5/5	delayed unable to walk in 4/5	ND
Delayed speech and language development	+	14/14	3/3	4/5	5/5 (none)	+
Muscular hypotonia	+	11/12	3/3	4/5	5/5	ND
Seizures	+	9/12	1/3	2/5	4/5	+
Apparent hypertelorism	+	+	3/3	1/2	5/5	ND
Long palpebral fissures	+	+	3/3	1/2		ND
Broad nasal tip	+	+	3/3	2/2	5/5	+
Tented upper lip vermilion	+	+	3/3	1/2	5/5	+
Brachytelephalangy	+	14/14	3/3	1/2	0/5	−
Anorectal abnormalities and/or constipation	−	6/12	3/3	1/2	ND	−
Aganglionic megacolon	−	2/14	1/3	1/2	ND	−
Heart defect	−	1/14	+	1/2	ND	−
Cleft palate	−	3/14	0/3	1/2	ND	−
Hearing impairment	+	3/14	0/3	1/2	ND	ND

ND, not described.

FACS analysis of granulocytes from our patient demonstrated severely decreased expression of GPI-APs. Functional analysis using *PIGL*-defective CHO cells revealed that the isoforms starting from the downstream methionines showed residual PIGL activity. It has been reported that two well-conserved motifs are essential for PIGL activity (Fig. 5B underlines). Two faint bands corresponding to the sizes of these isoforms were detected by western blot; the bigger band had both motifs but not the N-terminal transmembrane region. These two translation start sites do not fit well with Kozak's rule; therefore, these isoforms were not detected in the wild-type cells.

Severely decreased expression of GPI-APs in granulocytes of the patient suggest that these mutations in *PIGL* are associated with decreased GPI biosynthesis. Previous studies showed that the disruption of *PIGL* caused lethality in Saccharomyces cerevisiae [Watanabe et al., 1999], suggesting that PIGL has been considered as the only enzyme to catalyze the second step of GPI biosynthesis in yeast. Although the disease mechanims remain unknown, it is possible that a truncated protein translated from the allele with c.254_255del or C-terminal protein isoforms shown in our functional analysis using CHO cells might have the minimal residual activity of PIGL.

In conclusion, we identified compound heterozygous deletions in *PIGL* in a patient with distinctive facial appearance, developmental delay, intellectual disability, brachytelephalangy, and hyperphosphatasia. The clinical features were similar to those of HPMRS caused by mutations in *PIGV*, *PIGO*, *PGAP2*, *PGAP3*, and *PIGW*. Our findings will broaden the clinical spectrum of disorders with defects in the GPI biosynthesis pathway.

ACKNOWLEDGMENTS

The authors thank the patient's family who participated in this study. We are grateful to Prof. Shinji Nakao (Kanazawa University, Japan) for his valuable discussion, Yoko Tateda, Kumi Kato, Riyo Takahashi, Miyuki Tsuda, Nozomi Koshita, Mami Kikuchi, Kiyotaka Kuroda, and Kana Miyanagi for their technical assistance. We also acknowledge the support of the Biomedical Research Core of Tohoku University Graduate School of Medicine. This work was supported by a grant of Research on Applying Health Technology provided by the Ministry of Health, Labor and Welfare of Japan to Y.Ma. and Y.A. and a Grant-in-Aid for Scientific Research from the Japan Society for the Promotion of Science (C: 25461535) to I.F. This work was supported by a Grant-in-Aid for Scientific Research from the Japan Society for the Promotion of Science (C: 23590363); the Takeda Science Foundation; a Grant-in-Aid for Scientific Research on Innovative Areas (Exploring molecular basis for brain diseases based on personal genomics) from the Ministry of Education, Culture, Sports, Science, and Technology of Japan (25129705) to Y.Mu. and T.K.

REFERENCES

Almeida AM, Murakami Y, Layton DM, Hillmen P, Sellick GS, Maeda Y, Richards S, Patterson S, Kotsianidis I, Mollica L, Crawford DH, Baker A, Ferguson M, Roberts I, Houlston R, Kinoshita T, Karadimitris A. 2006. Hypomorphic promoter mutation in PIGM causes inherited glycosylphosphatidylinositol deficiency. Nat Med 12:846–851.

Chiyonobu T, Inoue N, Morimoto M, Kinoshita T, Murakami Y. 2014. Glycosylphosphatidylinositol (GPI) anchor deficiency caused by mutations in PIGW is associated with West syndrome and hyperphosphatasia with mental retardation syndrome. J Med Genet 51:203–207.

Fujita M, Kinoshita T. 2012. GPI-anchor remodeling: Potential functions of GPI-anchors in intracellular trafficking and membrane dynamics. Biochim Biophys Acta 1821:1050–1058.

Hansen L, Tawamie H, Murakami Y, Mang Y, ur Rehman S, Buchert R, Schaffer S, Muhammad S, Bak M, Nothen MM, Bennett EP, Maeda Y, Aigner M, Reis A, Kinoshita T, Tommerup N, Baig SM, Abou Jamra R. 2013. Hypomorphic mutations in PGAP2, encoding a GPI-anchor-remodeling protein, cause autosomal-recessive intellectual disability. Am J Hum Genet 92:575–583.

Horn D, Krawitz P, Mannhardt A, Korenke GC, Meinecke P. 2011. Hyperphosphatasia-mental retardation syndrome due to PIGV mutations: Expanded clinical spectrum. Am J Med Genet Part A 155A:1917–1922.

Howard MF, Murakami Y, Pagnamenta AT, Daumer-Haas C, Fischer B, Hecht J, Keays DA, Knight SJ, Kolsch U, Kruger U, Leiz S, Maeda Y, Mitchell D, Mundlos S, Phillips JA 3rd, Robinson PN, Kini U, Taylor JC, Horn D, Kinoshita T, Krawitz PM. 2014. Mutations in PGAP3 impair GPI-anchor maturation, causing a subtype of hyperphosphatasia with mental retardation. Am J Hum Genet 94:278–287.

Johnston JJ, Gropman AL, Sapp JC, Teer JK, Martin JM, Liu CF, Yuan X, Ye Z, Cheng L, Brodsky RA, Biesecker LG. 2012. The phenotype of a germline mutation in PIGA: The gene somatically mutated in paroxysmal nocturnal hemoglobinuria. Am J Hum Genet 90:295–300.

Krawitz PM, Schweiger MR, Rödelsperger C, Marcelis C, Kölsch U, Meisel C, Stephani F, Kinoshita T, Murakami Y, Bauer S, Isau M, Fischer A, Dahl A, Kerick M, Hecht J, Köhler S, Jäger M, Grünhagen J, de Condor BJ, Doelken S, Brunner HG, Meinecke P, Passarge E, Thompson MD, Cole DE, Horn D, Roscioli T, Mundlos S, Robinson PN. 2010. Identity-by-descent filtering of exome sequence data identifies PIGV mutations in hyperphosphatasia mental retardation syndrome. Nat Genet 42:827–829.

Krawitz Peter M, Murakami Y, Hecht J, Krüger J, Holder U, Susan E, Mortier Geert, Delle Chiaie, De Baere E, Thompson Miles D, Roscioli T, Kielbasa S, Kinoshita T, Mundlos S, Robinson Peter N, Horn D. 2012. Mutations in PIGO, a member of the GPI-anchor-synthesis pathway, cause hyperphosphatasia with mental retardation. Am J Hum Genet 91:146–151.

Krawitz PM, Murakami Y, Riess A, Hietala M, Kruger U, Zhu N, Kinoshita T, Mundlos S, Hecht J, Robinson PN, Horn D. 2013. PGAP2 mutations, affecting the GPI-anchor-synthesis pathway, cause hyperphosphatasia with mental retardation syndrome. Am J Hum Genet 92:584–589.

Kruse K, Hanefeld F, Kohlschutter A, Rosskamp R, Gross-Selbeck G. 1988. Hyperphosphatasia with mental retardation. J Pediatr 112:436–439.

Kvarnung M, Nilsson D, Lindstrand A, Korenke GC, Chiang SC, Blennow E, Bergmann M, Stodberg T, Makitie O, Anderlid BM, Bryceson YT, Nordenskjold M, Nordgren A. 2013. A novel intellectual disability syndrome caused by GPI anchor deficiency due to homozygous mutations in PIGT. J Med Genet 50:521–528.

Mabry CC, Bautista A, Kirk RF, Dubilier LD, Braunstein H, Koepke JA. 1970. Familial hyperphosphatase with mental retardation, seizures, and neurologic deficits. J Pediatr 77:74–85.

Maydan G, Noyman I, Har-Zahav A, Neriah ZB, Pasmanik-Chor M, Yeheskel A, Albin-Kaplanski A, Maya I, Magal N, Birk E, Simon AJ, Halevy A, Rechavi G, Shohat M, Straussberg R, Basel-Vanagaite L. 2011. Multiple congenital anomalies-hypotonia-seizures syndrome is caused by a mutation in PIGN. J Med Genet 48:383–389.

McKenna A, Hanna M, Banks E, Sivachenko A, Cibulskis K, Kernytsky A, Garimella K, Altshuler D, Gabriel S, Daly M, DePristo MA. 2010. The Genome Analysis Toolkit: A MapReduce framework for analyzing next-generation DNA sequencing data. Genome Res 20:1297–1303.

Murakami Y, Kanzawa N, Saito K, Krawitz PM, Mundlos S, Robinson PN, Karadimitris A, Maeda Y, Kinoshita T. 2012. Mechanism for release of alkaline phosphatase caused by glycosylphosphatidylinositol deficiency in patients with hyperphosphatasia mental retardation syndrome. J Biol Chem 287:6318–6325.

Nakamura N, Inoue N, Watanabe R, Takahashi M, Takeda J, Stevens VL, Kinoshita T. 1997. Expression cloning of PIG-L, a candidate N-acetylglucosaminyl-phosphatidylinositol deacetylase. J Biol Chem 272:15834–15840.

Nakamura K, Osaka H, Murakami Y, Anzai R, Nishiyama K, Kodera H, Nakashima M, Tsurusaki Y, Miyake N, Kinoshita T, Matsumoto N, Saitsu H. 2014. PIGO mutations in intractable epilepsy and severe developmental delay with mild elevation of alkaline phosphatase levels. Epilepsia 55:e13–17.

Ng Bobby G, Hackmann K, Jones Melanie A, Eroshkin Alexey M, He P, Wiliams R, Bhide S, Cantagrel V, Gleeson Joseph G, Paller Amy S, Schnur Rhonda E, Tinschert S, Zunich J, Hegde Madhuri R, Freeze Hudson H. 2012. Mutations in the glycosylphosphatidylinositol gene PIGL cause CHIME syndrome. Am J Hum Genet 90:685–688.

Ohba C, Okamoto N, Murakami Y, Suzuki Y, Tsurusaki Y, Nakashima M, Miyake N, Tanaka F, Kinoshita T, Matsumoto N, Saitsu H. 2014. PIGN mutations cause congenital anomalies, developmental delay, hypotonia, epilepsy, and progressive cerebellar atrophy. Neurogenetics 15:85–92.

Schnur RE, Greenbaum BH, Heymann WR, Christensen K, Buck AS, Reid CS. 1997. Acute lymphoblastic leukemia in a child with the CHIME neuroectodermal dysplasia syndrome. Am J Med Genet 72:24–29.

Shashi V, Zunich J, Kelly TE, Fryburg JS. 1995. Neuroectodermal (CHIME) syndrome: An additional case with long term follow up of all reported cases. J Med Genet 32:465–469.

Wang K, Li M, Hakonarson H. 2010. ANNOVAR: Functional annotation of genetic variants from high-throughput sequencing data. Nucleic Acids Res 38:e164.

Ware RE, Rosse WF, Howard TA. 1994. Mutations within the Piga gene in patients with paroxysmal nocturnal hemoglobinuria. Blood 83:2418–2422.

Watanabe R, Ohishi K, Maeda Y, Nakamura N, Kinoshita T. 1999. Mammalian PIG-L and its yeast homologue Gpi12p are N-acetylglucosaminylphosphatidylinositol de-N-acetylases essential in glycosylphosphatidylinositol biosynthesis. Biochem J 339:185–192.

Post-Golgi anterograde transport requires GARP-dependent endosome-to-TGN retrograde transport

Tetsuya Hirata[a,b,*], Morihisa Fujita[c,*], Shota Nakamura[a], Kazuyoshi Gotoh[a], Daisuke Motooka[a], Yoshiko Murakami[a,b], Yusuke Maeda[a,b], and Taroh Kinoshita[a,b]

[a]Research Institute for Microbial Diseases and [b]WPI Immunology Frontier Research Center, Osaka University, Osaka 565-0871, Japan; [c]Key Laboratory of Carbohydrate Chemistry and Biotechnology, Ministry of Education, School of Biotechnology, Jiangnan University, Wuxi, Jiangsu 214122, China

ABSTRACT **The importance of endosome-to–*trans*-Golgi network (TGN) retrograde transport in the anterograde transport of proteins is unclear. In this study, genome-wide screening of the factors necessary for efficient anterograde protein transport in human haploid cells identified subunits of the Golgi-associated retrograde protein (GARP) complex, a tethering factor involved in endosome-to-TGN transport. Knockout (KO) of each of the four GARP subunits, VPS51–VPS54, in HEK293 cells caused severely defective anterograde transport of both glycosylphosphatidylinositol (GPI)-anchored and transmembrane proteins from the TGN. Overexpression of VAMP4, v-SNARE, in VPS54-KO cells partially restored not only endosome-to-TGN retrograde transport, but also anterograde transport of both GPI-anchored and transmembrane proteins. Further screening for genes whose overexpression normalized the VPS54-KO phenotype identified TMEM87A, encoding an uncharacterized Golgi-resident membrane protein. Overexpression of TMEM87A or its close homologue TMEM87B in VPS54-KO cells partially restored endosome-to-TGN retrograde transport and anterograde transport. Therefore GARP- and VAMP4-dependent endosome-to-TGN retrograde transport is required for recycling of molecules critical for efficient post-Golgi anterograde transport of cell-surface integral membrane proteins. In addition, TMEM87A and TMEM87B are involved in endosome-to-TGN retrograde transport.**

Monitoring Editor
Robert G. Parton
University of Queensland

Received: Nov 26, 2014
Revised: Jun 22, 2015
Accepted: Jul 2, 2015

This article was published online ahead of print in MBoC in Press (http://www.molbiolcell.org/cgi/doi/10.1091/mbc.E14-11-1568) on July 8, 2015.

*These authors contributed equally.

Address correspondence to: Taroh Kinoshita (tkinoshi@biken.osaka-u.ac.jp), Morihisa Fujita (fujita@jiangnan.edu.cn).

Abbreviations used: BSD, blasticidin-S deaminase; CHX, cycloheximide; COG, conserved oligomeric Golgi; CRISPR, clustered, regularly interspaced, short palindromic repeat; CTxB, cholera toxin B subunit; Dox, doxycycline; GARP, Golgi-associated retrograde protein; GPCR, G protein–coupled receptor; GPI-AP, glycosylphosphatidylinositol-anchored protein; PI-PLC, phosphatidylinositol-specific phospholipase C; Pur, puromycin *N*-acetyl-transferase; RFP, red fluorescent protein; VPS, vacuolar protein sorting; VSVG, vesicular stomatitis virus G protein.

INTRODUCTION

Protein trafficking in eukaryotic cells is mediated by bidirectional vesicular transport between cellular compartments (Brandizzi and Barlowe, 2013). Vesicular transport can be divided into two pathways: anterograde transport, which is the route from the endoplasmic reticulum (ER) to the plasma membrane, and retrograde transport, which is the opposite route. Each of these transport pathways consists of four steps: budding, movement, tethering, and uncoating and fusion (Bonifacino and Glick, 2004; Brandizzi and Barlowe, 2013). Anterograde transport from the ER to the ER–Golgi intermediate compartment is mediated by COPII-coated vesicles, and retrograde transport from the Golgi to the ER is mediated by COPI-coated vesicles. Inhibition of COPI-dependent retrograde transport disrupts COPII-mediated anterograde transport because recycling proteins, including vesicle–soluble *N*-ethylmaleimide–sensitive factor attachment protein receptors (v-SNAREs) and

Supplemental Material can be found at:
http://www.molbiolcell.org/content/suppl/2015/07/06/mbc.E14-11-1568v1.DC1.html

cargo receptors in the ER, are depleted (Pepperkok *et al.*, 1993; Peter *et al.*, 1993). Therefore protein recycling mediated by COPI-dependent retrograde transport is required for efficient anterograde transport. Anterograde and retrograde transport also take place between the TGN and the plasma membrane. Three retrograde transport pathways to the TGN have been identified: from early, recycling, and late endosomes (Chia *et al.*, 2013). Retrograde transport carriers from early or recycling endosomes contain the v-SNARE vesicle-associated membrane protein 3 (VAMP3) or VAMP4. Fusion with the TGN membrane is mediated by SNARE complex assembly between VAMP4 and the TGN-localized target (t)-SNAREs syntaxin 6 (STX6), STX16, and Vti1 (Mallard *et al.*, 2002; Hong and Lev, 2013). Retrograde transport to the TGN was first discovered through the transport routes of toxins (Mallard *et al.*, 1998) and is now believed to act as a protein-recycling route from endosomes.

Previous studies showed that secretion of Wnt is dependent on endosome-to-TGN retrograde transport, based on the necessary recycling of its cargo receptor, wntless (Belenkaya *et al.*, 2008; Franch-Marro *et al.*, 2008; Harterink *et al.*, 2011). These results highlighted the importance of protein recycling from endosomes. However, other studies showed that anterograde transport of thermosensitive vesicular stomatitis virus G protein ($VSVG^{tsO45}$, hereafter $VSVG^{ts}$), which is more widely used as a model protein for testing anterograde transport, is not impaired in cells depleted of SNARE proteins involved in endosome-to-TGN retrograde transport (Choudhury *et al.*, 2006; Nishimoto-Morita *et al.*, 2009; Shitara *et al.*, 2013). These results were quite different from the case of Wnt secretion and suggested that protein recycling to the TGN is less important for the anterograde transport of $VSVG^{ts}$. Therefore the relevance of endosome-to-TGN retrograde transport in the anterograde transport of various cargoes needs to be clarified.

Glycosylphosphatidylinositol (GPI) addition is a highly conserved posttranslational modification in eukaryotic cells and is used in the anchoring of proteins (Kinoshita *et al.*, 2008). In mammalian cells, ~150 proteins are anchored to the plasma membrane via GPI. The synthesis of GPI in the ER is followed by its transfer to proteins, generating immature GPI-anchored proteins (GPI-APs) in which GPI is then structurally remodeled by post-GPI attachment to proteins 1 (PGAP1) and PGAP5 (Tanaka *et al.*, 2004; Fujita *et al.*, 2009). Because structural remodeling is important for interaction with the p24 family complex, a cargo receptor of GPI-APs, the PGAP1 or PGAP5 mutant cells exhibit delayed anterograde transport of GPI-APs from the ER (Fujita *et al.*, 2011). However, little is known about the molecular mechanism of post-Golgi anterograde transport of GPI-APs.

In this study, we carried out haploid genetic screening to identify genes necessary for the efficient anterograde transport of GPI-APs and thereby identified genes encoding subunits of the Golgi-associated retrograde protein (GARP) complex. The GARP complex is a multisubunit tethering factor localized in the TGN and involved in endosome-to-TGN retrograde transport (Bonifacino and Hierro, 2011). It is composed of four subunits—vacuolar protein sorting 51 (VPS51), VPS52, VPS53, and VPS54—each of which is essential for tethering (Conibear and Stevens, 2000; Siniossoglou and Pelham, 2002; Perez-Victoria *et al.*, 2008, 2010a). Here we demonstrate that the GARP- and VAMP4-dependent endosome-to-TGN retrograde transport is required for recycling of factors necessary for the efficient post-Golgi anterograde transport of cell-surface integral membrane proteins such as GPI-anchored or transmembrane proteins.

RESULTS

Screening mutant haploid cells defective in GPI-AP transport

To identify genes necessary for the efficient anterograde transport of GPI-APs, we performed genetic screening in human haploid cells (HAP1; Carette *et al.*, 2011b), using a GPI-anchored reporter protein to monitor the transport of GPI-APs previously developed in genetic screening with CHO cells (Maeda *et al.*, 2008; Fujita *et al.*, 2009). This reporter is a chimeric protein consisting of a luminal domain of $VSVG^{ts}$, a FLAG tag, an enhanced green fluorescent protein (EGFP), and a C-terminal GPI attachment signal (VFG-GPI). $VSVG^{ts}$ causes accumulation of the reporter in the ER at the restrictive temperature of 40°C because of the protein's unfolding status and allows synchronized exit from the ER after rapid folding at the permissive temperature of 32°C. Therefore transport status at *x* minutes after the temperature shift can be measured by determining the ratio of surface (cell-surface FLAG tag determined by flow cytometry) to total (fluorescence of EGFP) VFG-GPI. Thus we first established a HAP1 cell line, HAP1FF9, with doxycycline (Dox)-inducible expression of VFG-GPI and mutagenized the cells using a retroviral gene-trapping vector. Control genomic DNA was extracted before the enrichment of transport mutants. Using a cell sorter, we collected mutant cells showing slow GPI-AP transport, as determined by decreased surface levels of VFG-GPI, 60 min after the temperature shift. The collected cells were cultured and then re-sorted to enrich mutants with delayed GPI-AP transport (sort 2, Figure 1A). Retroviral insertion sites in the genomic DNA from sort 2 cells and control, pre-enrichment cells were analyzed by deep sequencing. Enrichment rates were calculated for the respective genes by comparing the numbers of mapped independent-insertion sites of the respective gene between sort 2 and control cells. The genes *PGAP1* and *PGAP5* (*MPPE1*), whose mutations have been known to cause delayed transport of GPI-APs, were enriched in sort 2 (Figure 1B and Supplemental Table S1), indicating the usefulness of the method. In addition, the *PGAP2* gene, which is required for GPI fatty acid remodeling in the Golgi (Tashima *et al.*, 2006), was also enriched in sort 2. In the *PGAP2* mutant cells, transport of GPI-APs is almost normal, but the surface expression of GPI-APs is greatly decreased because lyso form GPI-APs, the intermediate forms during the fatty acid remodeling, which harbor only a single acyl chain, are not reacylated due to the PGAP2 defect and are released easily from the membrane into medium soon after arrival at the cell surface.

Knockout of GARP complex subunits severely impairs anterograde transport of proteins

Three genes—*C11orf2* (also known as *VPS51* or *Ang2*), *VPS52*, and *VPS54*, encoding subunits of the GARP complex, a tethering factor—were significantly enriched in sort 2 cells ($p < 0.01$), and the fourth subunit—VPS53—was positioned close to the significance limit (Figure 1B and Supplemental Table S1). In addition, the *COG8* gene, encoding a subunit of conserved oligomeric Golgi (COG) complex, another multisubunit tethering factor, was highly enriched. To investigate whether the GARP complex is involved in the anterograde transport of GPI-APs, we generated GARP-KO cells using the clustered, regularly interspaced, short palindromic repeat (CRISPR)–Cas9 system (Cong *et al.*, 2013; Mali *et al.*, 2013) in HEK293FF6 cells, bearing Dox-inducible VFG-GPI. All mutations caused frameshifts (Supplemental Table S2), indicating that all mutant cells had completely lost expression of the targeted genes. Indeed, VPS52 and VPS53 proteins nearly completely disappeared in V52KO and V53KO cells, respectively (Figure 2A). To compare the kinetics of anterograde transport of VFG-GPI, we conducted a transport assay

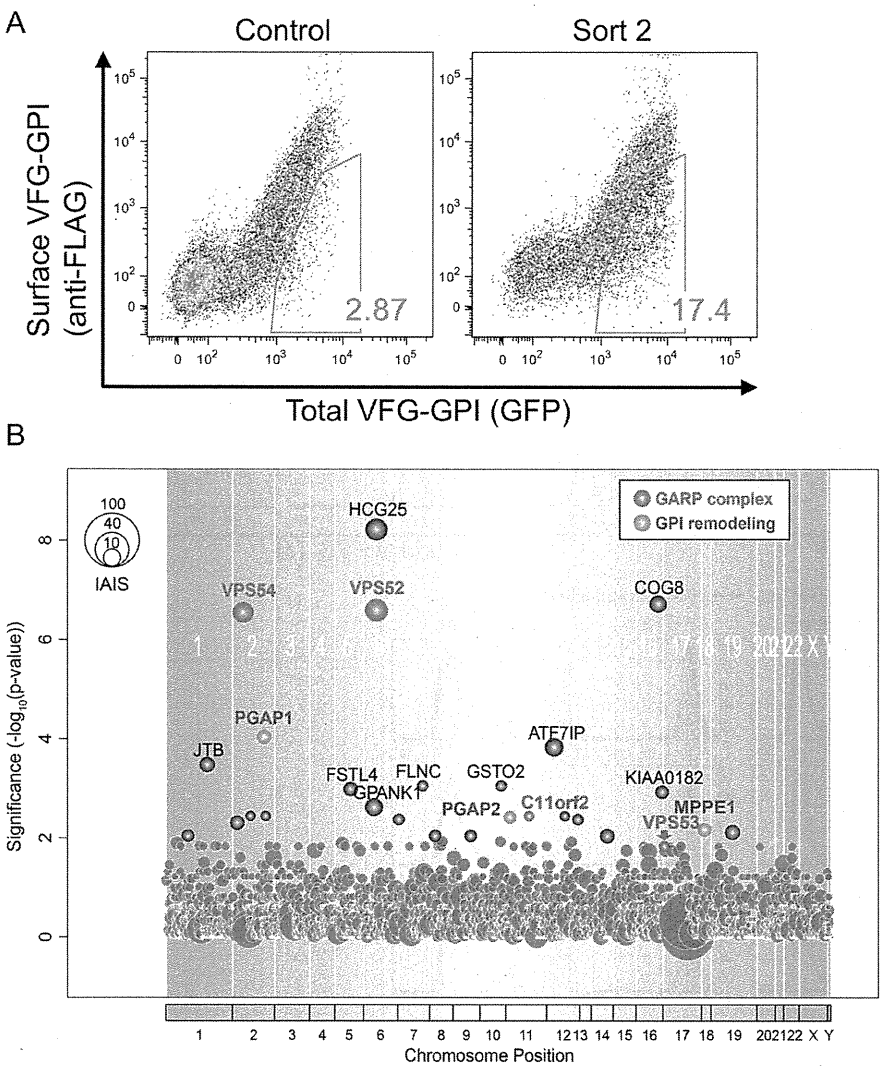

FIGURE 1: Haploid genetic screening of the factors required for the anterograde transport of GPI-APs. (A) Transport assay of VFG-GPI in HAP1FF9 wild-type cells (left) and the enriched cell population after sorting twice for delayed transport (right). (B) The significance of the enrichment of gene-trap insertions in an enriched population with delayed transport compared with the nonselected population was calculated and plotted as a bubble plot. The horizontal line shows the chromosomal position of the genes, and the vertical line shows the significance of enrichment of each gene (p value). The size of the bubble shows the number of inactivated insertion sites. Genes significantly enriched in sort 2 ($p < 0.01$) are colored. Red bubbles, genes encoding the GARP complex subunit; green bubbles, genes involved in GPI-AP remodeling. The bubble of VPS53 indicated by an arrow was close to the significance limit.

using HEK293FF6 wild-type or GARP-KO cells. The relative expression of VFG-GPI in each KO cell line (V51KO, V52KO, V53KO, and V54KO) 90 min after the temperature shift was 14.7 ± 5.2, 21.7 ± 11.0, 5.9 ± 1.7, and 27.0 ± 3.5%, respectively (mean ± SD; Figure 2, B and C), suggesting that the anterograde transport of GPI-APs is severely impaired in GARP-KO cells. Note that the surface expression of VFG-GPI at 0 min was lower in GARP-KO cells than in wild-type cells, consistent with the delayed transport occurring from the very beginning in KO cells. To investigate whether delayed transport was specific to GPI-APs, we conducted a similar transport assay of a transmembrane-type reporter protein in GARP-KO cells. The reporter protein, FVG-TM, was a chimeric protein consisting of a FLAG tag, VSVG^{ts} (full length), and EGFP (Maeda *et al.*, 2008; Fujita *et al.*, 2009). Because the HEK293FF6 cell line does not have FVG-TM, its expression plasmid was transiently transfected into cells and its transport then assayed. After 90 min, the relative expression of FVG-TM in V51KO, V52KO, V53KO, and V54KO cells was only 3.7 ± 0.95, 8.0 ± 2.5, 2.4 ± 1.3, and 18.6 ± 7.0%, respectively (mean ± SD; Figure 2, D and E). Expression of the responsible gene in each KO cell restored the delayed transport of both VFG-GPI and FVG-TM (Figure 2F), thus ruling out off-target effects. These results indicated that the GARP complex is required for the efficient anterograde transport of both GPI-anchored and transmembrane proteins.

Post-Golgi anterograde transport is defective in V54KO cells

The step in anterograde transport that is affected by a defect in the GARP complex was identified using confocal microscopy in cells stably transfected with an empty vector or VPS54 (V54KO+Vec or V54KO+VPS54), together with red fluorescent protein (RFP)–GPP34 as a TGN marker. VFG-GPI transport was chased for the indicated time, after which the cells were fixed to terminate the transport. Ratios of VFG-GPI fluorescence intensity in the TGN to total cellular VFG-GPI fluorescence intensity were determined at each time point (Figure 3B). In V54KO+VPS54 cells, the amount of VFG-GPI that reached the TGN gradually increased for 20 min, remained constant for the next 60 min, and then finally decreased at 90 min (Figure 3, A and B), suggesting that after VFG-GPI reached the TGN, it was transported to the cell surface. In V54KO+Vec cells, the relative intensity in TGN was slightly increased at 20 min but further increased for the next 60 min (Figure 3, A and B), suggesting that after its arrival at the TGN, VFG-GPI accumulated in the TGN for at least 60 min. This result suggested that GARP complex is required for post-Golgi transport. Although ER-to-Golgi transport appeared to be slightly impaired in V54KO+Vec cells (0.15 ± 0.012 vs. 0.095 ± 0.0089 at 20 min; mean ± SEM), this might have been because of the indirect effect of impaired post-Golgi transport. To confirm that post-Golgi anterograde transport is impaired in V54KO cells, we allowed VFG-GPI to accumulate in the Golgi by culturing cells at restrictive temperature of 19°C and then synchronously releasing them by a temperature shift to 32°C. VFG-GPI that reached the cell surface was stained with anti-FLAG antibody under nonpermeabilized conditions. Ratios of VFG-GPI fluorescence intensity in the cell surface to total cellular VFG-GPI fluorescence intensity were quantified (Figure 3D). As shown in Figure 3C, at 0 min, most of the VFG-GPI was localized in the TGN in both V54KO+VPS54 and V54KO+Vec cells. By 45 min, although a large amount of the VFG-GPI reached the cell surface in

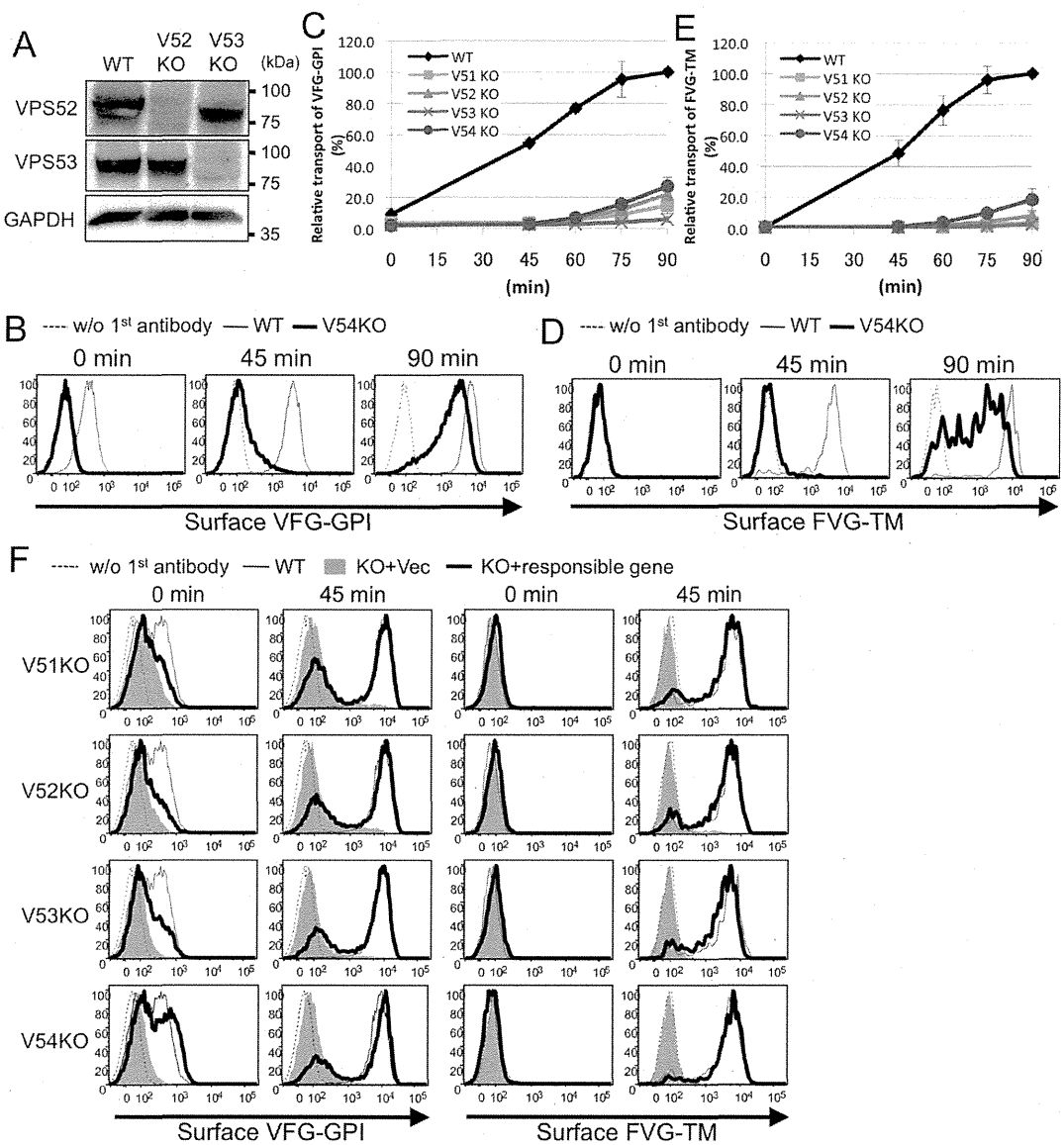

FIGURE 2: Knockout (KO) of GARP complex subunits severely impairs the anterograde transport of proteins. (A) Western blotting of VPS52 and VPS53 in HEK293FF6 wild-type (WT), VPS52-KO (V52KO), and VPS53-KO (V53KO) cells, showing nearly complete reduction by specific knockout. GAPDH was used as a loading control. (B) Transport assay of VFG-GPI in wild-type (WT) and GARP-KO cells. Surface expression of VFG-GPI at the indicated time in WT and VPS54-KO (V54KO) cells is shown as an example. (C) Relative transport of VFG-GPI in GARP-KO cells. The geometric mean fluorescence of surface VFG-GPI, as shown in the histograms in B, was quantified for each time point, plotting the geometric mean of WT cells at 90 min as 100% relative transport. (D) Transport assay of FVG-TM in WT and GARP-KO cells. WT and GARP-KO cells were transiently transfected with FVG-TM. Surface expression of FVG-TM at the indicated time in WT and V54KO cells is shown as an example. (E) Relative transport of FVG-TM. The geometric mean fluorescence of surface FVG-TM, as shown in the histograms in D, was quantified similarly to C. (F) Rescue of transport delay in GARP-KO cells by the expression of the responsible genes. GARP-KO cells were transiently transfected with a VPS51, VPS52, VPS53, or VPS54 expression plasmid, after which the transport of VFG-GPI (left) was analyzed. For FVG-TM transport, cells were cotransfected with FVG-TM and indicated genes. The quantitative data are the means of three independent experiments. Error bars represent the SDs ($n = 3$).

V54KO+VPS54 cells (Figure 3, C and D), this was barely the case in V54KO+Vec cells, as VFG-GPI largely remained in the TGN (Figure 3, C and D). This result strongly suggested requirement of the GARP complex in post-Golgi anterograde transport. From these results, we concluded that the GARP complex is required for efficient post-Golgi anterograde transport.

CD59, an endogenous GPI-AP, was missorted to lysosomes in V54KO cells

The fact that post-Golgi anterograde transport was impaired in V54KO cells led us to investigate whether the cargo sorting at the TGN was impaired. To elucidate this point, we analyzed intracellular localization of endogenous GPI-AP, CD59. To eliminate cell-surface

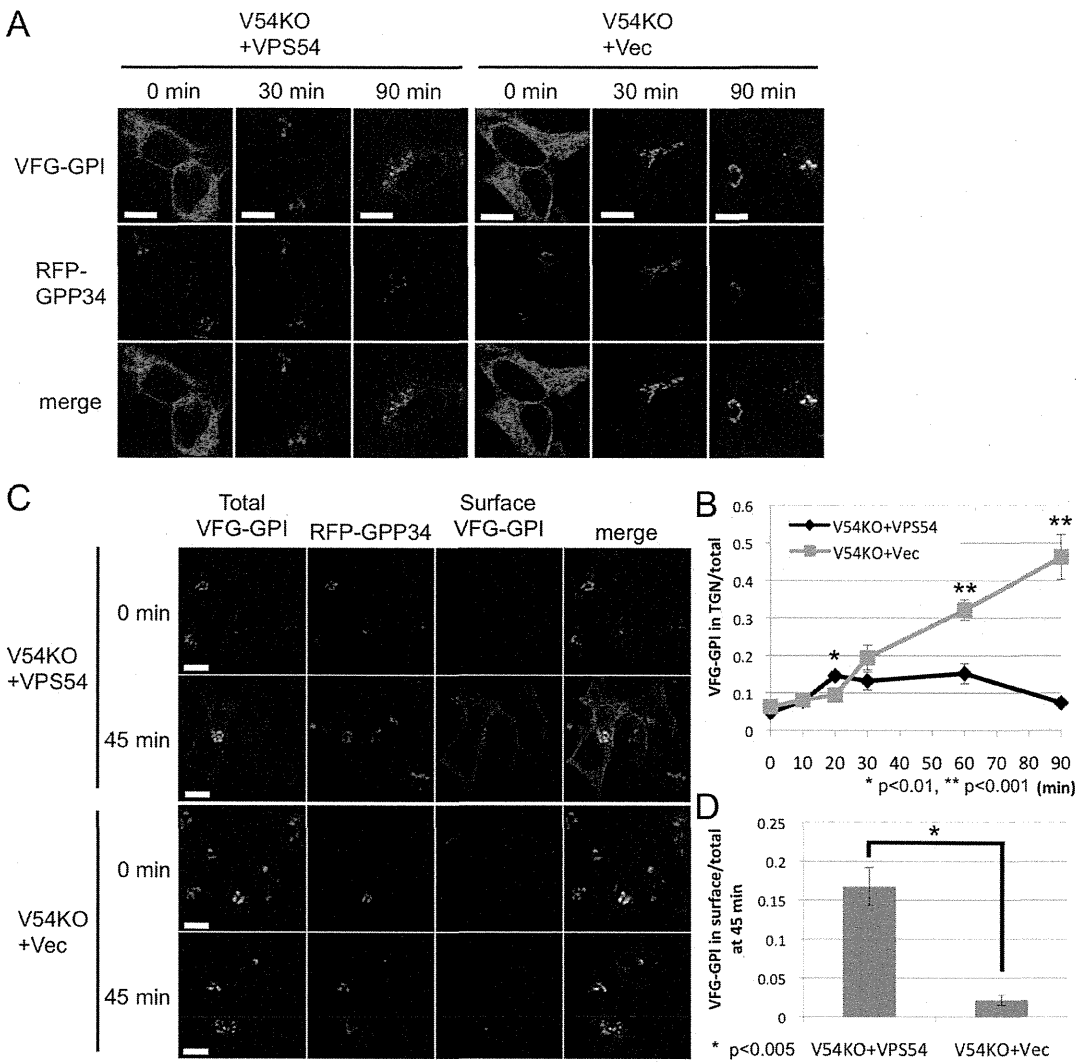

FIGURE 3: Post-Golgi anterograde transport is defective in V54KO cells. (A) VFG-GPI transport from the ER in V54KO or restored cells. Cells were cultured in medium containing 1 μg/ml Dox at 40°C for 24 h. VFG-GPI transport was chased at 32°C for the indicated time in medium containing 100 μg/ml CHX. Images at 0, 30, and 90 min. Green, VFG-GPI; red, RFP-GPP34 as a TGN marker. Scale bars, 10 μm. (B) The TGN localization of VFG-GPI was quantified based on A. The ratio of the VFG-GPI intensity in the TGN to the total fluorescence intensity was determined. Data are the means of 10 independent images. Error bars represent the SEM ($n = 10$). Similar results were obtained from two independent experiments. (C) Post-Golgi transport of VFG-GPI in V54KO or restored cells. Cells cultured in medium containing 1 μg/ml Dox for 24 h at 40°C were precultured in medium containing 100 μg/ml CHX for 3 h at 19°C, after which VFG-GPI transport was chased at 32°C for 0 or 45 min. To detect surface VFG-GPI, cells were stained with anti-FLAG M2 antibody under nonpermeabilized conditions. Green, total expression of VFG-GPI; red, RFP-GPP34; cyan, surface expression of VFG-GPI. Scale bars, 10 μm. Similar results were obtained from two independent experiments. (D) The ratio of surface arrived VFG-GPI was quantified based on C. Data are the means of five independent images. Error bars represent the SEM ($n = 5$). Similar results were obtained from two independent experiments.

CD59, we treated cells with phosphatidylinositol-specific phospholipase C (PI-PLC) before fixation and analyzed them by confocal microscopy. In V54KO+VPS54 cells, CD59 was hardly detectable, whereas many CD59-positive vesicles were observed in V54KO+Vec cells (Figure 4A). These vesicles were largely colocalized with LAMP1 but not with EEA1 (Figure 4, A and B). This result suggested that CD59 was missorted to lysosomes in V54KO cells probably due to defective post-Golgi anterograde transport. If most of the GPI-APs are missorted to lysosomes and degraded, it is possible that surface expression of GPI-APs is reduced. However, flow cytometric analysis revealed that surface expression of CD59 was not reduced in V54KO+Vec cells compared with V54KO+VPS54 cells (Supplemental Figure S1), suggesting that the majority of GPI-APs are properly but slowly transported to the cell surface.

VAMP4-mediated retrograde transport is required for recycling of proteins critical for efficient anterograde transport

The GARP complex tethers endosome-derived transport carriers to the TGN, so endosome-to-TGN retrograde transport might contribute to post-Golgi anterograde transport by recycling the molecules involved. Thus, in V54KO cells, fewer of these molecules, such as

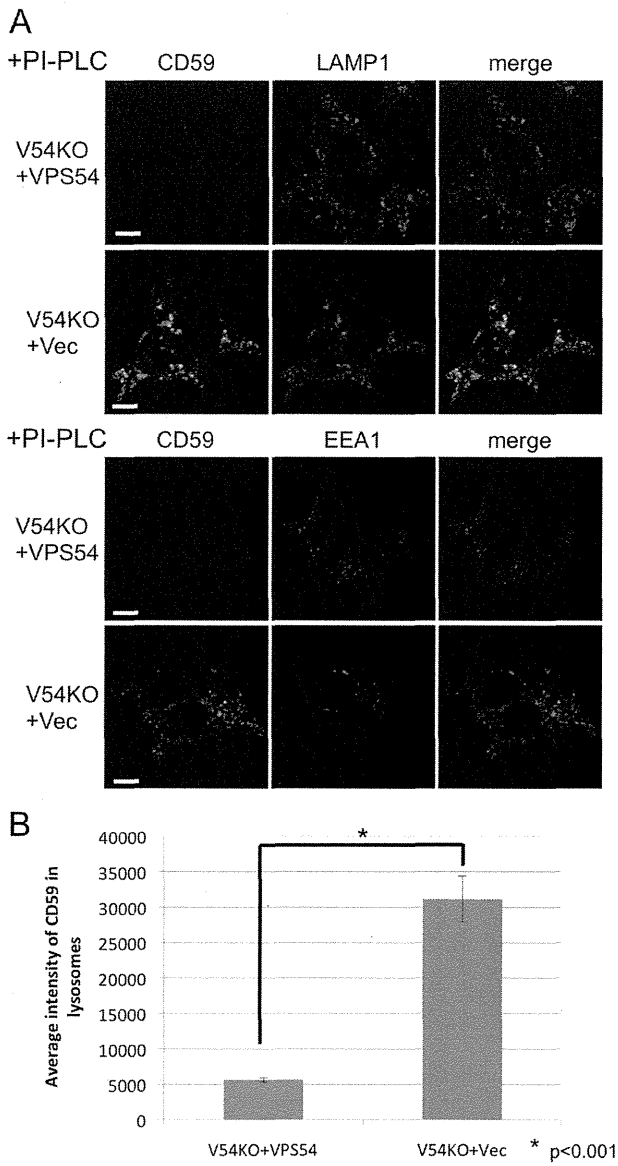

FIGURE 4: Missorting of CD59 to lysosomes in V54KO cells. (A) Intracellular localization of endogenous GPI-AP, CD59. Cells were treated with PI-PLC at 37°C for 1.5 h, after which they were fixed and double-stained with anti-CD59 and anti-LAMP1 or anti-EEA1. Green, CD59; red, LAMP1 (top) and EEA1 (bottom) as lysosome and early-endosome markers, respectively. Scale bars, 10 μm. (B) CD59 localized in lysosomes was quantified from the images of A. Data are the means of 10 independent images. Error bars represent the SEM ($n = 10$). Similar results were obtained in two independent experiments.

SNARE proteins, would be found in their expected location. To examine this possibility, we overexpressed several SNARE proteins localized in the post-Golgi compartments in V54KO cells and then assessed restoration of anterograde transport . Overexpression of VAMP4 partially restored the delayed transport of both VFG-GPI and FVG-TM, whereas overexpression of VAMP2, VAMP3, VAMP7, STX1A, or STX6 did not (Figure 5A and Supplemental Figure S2A). To investigate the mechanism by which VAMP4 overexpression restored anterograde transport in V54KO cells, we analyzed plasma membrane–to-TGN retrograde transport using the cholera toxin B subunit (CTxB) as cargo. We prepared V54KO cells stably expressing VAMP4 (V54KO+VAMP4) and collected cells that restored anterograde transport of VFG-GPI (Supplemental Figure S2B). To assess CTxB retrograde transport, we bound Alexa 488–conjugated CTxB to the cell surface at 4°C, after which we incubated cells at 37°C for 60 min to allow the transport of CTxB. Because CTxB binding to the cell surface was decreased in V54KO cells (Supplemental Figure S2C), retrograde transport efficiency was determined by comparing the ratio of Golgi-associated CTxB to total CTxB. The ratio of CTxB localized in the TGN at 60 min in V54KO+Vec cells was lower than that in V54KO+VPS54 cells (Figure 5, B and C), indicating the impairment of endosome-to-TGN retrograde transport in V54KO cells, consistent with the findings of a previous study (Perez-Victoria *et al.*, 2008). As shown in Figure 5, B and C, the amount of TGN-localized CTxB at 60 min was clearly higher in V54KO+VAMP4 cells than in V54KO+Vec cells (0.21 ± 0.024 vs. 0.15 ± 0.016; mean ± SEM). We interpreted these data as indicating that retrograde transport of CTxB was partially restored by VAMP4 overexpression and that the statistical insignificance ($p = 0.055$) may be accounted for by the presence in V54KO+VAMP4 cells of a population that did not restore the anterograde transport (Supplemental Figure S2B). These results and those on the restoration of anterograde transport strongly indicated that VAMP4-mediated retrograde transport is important for the recycling of molecules involved in the anterograde transport of both GPI-anchored and transmembrane proteins. This conclusion was confirmed by using small interfering RNA (siRNA) to abolish the expression of VAMP4 or STX6. For this experiment, we used a HEK293FF6 cell line for VFG-GPI transport and a HEK293TM10 cell line, in which expression of FVG-TM could be induced with Dox. As shown in Figure 5D, expression of both STX6 and VAMP4 was efficiently knocked down. Depletion of VAMP4 or STX6 impaired the anterograde transport of both VFG-GPI and FVG-TM (Figure 5E). These results complemented those from the VAMP4-overexpression experiments. We concluded that GARP- and VAMP4-mediated retrograde transport is required for recycling the factors necessary for the post-Golgi anterograde transport of both GPI-anchored and transmembrane proteins.

Potential role for TMEM87A and TMEM87B in endosome-to-TGN retrograde transport

We reasoned that overexpression of a protein involved in VAMP4-mediated endosome-to-TGN retrograde transport would rescue the V54KO transport defect. Therefore we next tried to isolate suppressor genes that, when overexpressed, rescued the transport delay in V54KO cells. A cDNA library derived from human brain was introduced into V54KO cells, and the cDNAs in the transport-restored cell populations were sequenced. From this screening, we obtained *TMEM87A*, a multipass transmembrane protein belonging to the LU7TM family (from Uniprot; Supplemental Table S3). Overexpression of TMEM87A partially restored the defect in anterograde transport of both VFG-GPI and FVG-TM in V54KO cells (Figure 6A; geometric means of cell surface levels of VFG-GPI and FVG-TM were 1.92 ± 0.22 and 4.45 ± 1.1 times, respectively, those in V54KO+Vec; $n = 3$). Overexpression of TMEM87B, a close homologue of TMEM87A and a member of the same family, also restored the defect in V54KO cells (Figure 6A; geometric means of cell surface levels of VFG-GPI and FVG-TM were 1.85 ± 0.22 and 3.42 ± 0.99 times, respectively, those in V54KO+Vec; $n = 3$), suggesting its functional redundancy with TMEM87A. Recently a role for GPR107—another LU7TM family member—was shown in retrograde transport of toxins such as exotoxin A of *Pseudomonas aeruginosa* and ricin (Carette *et al.*, 2011a; Elling *et al.*, 2011; Tafesse *et al.*, 2014; Zhou *et al.*, 2014).

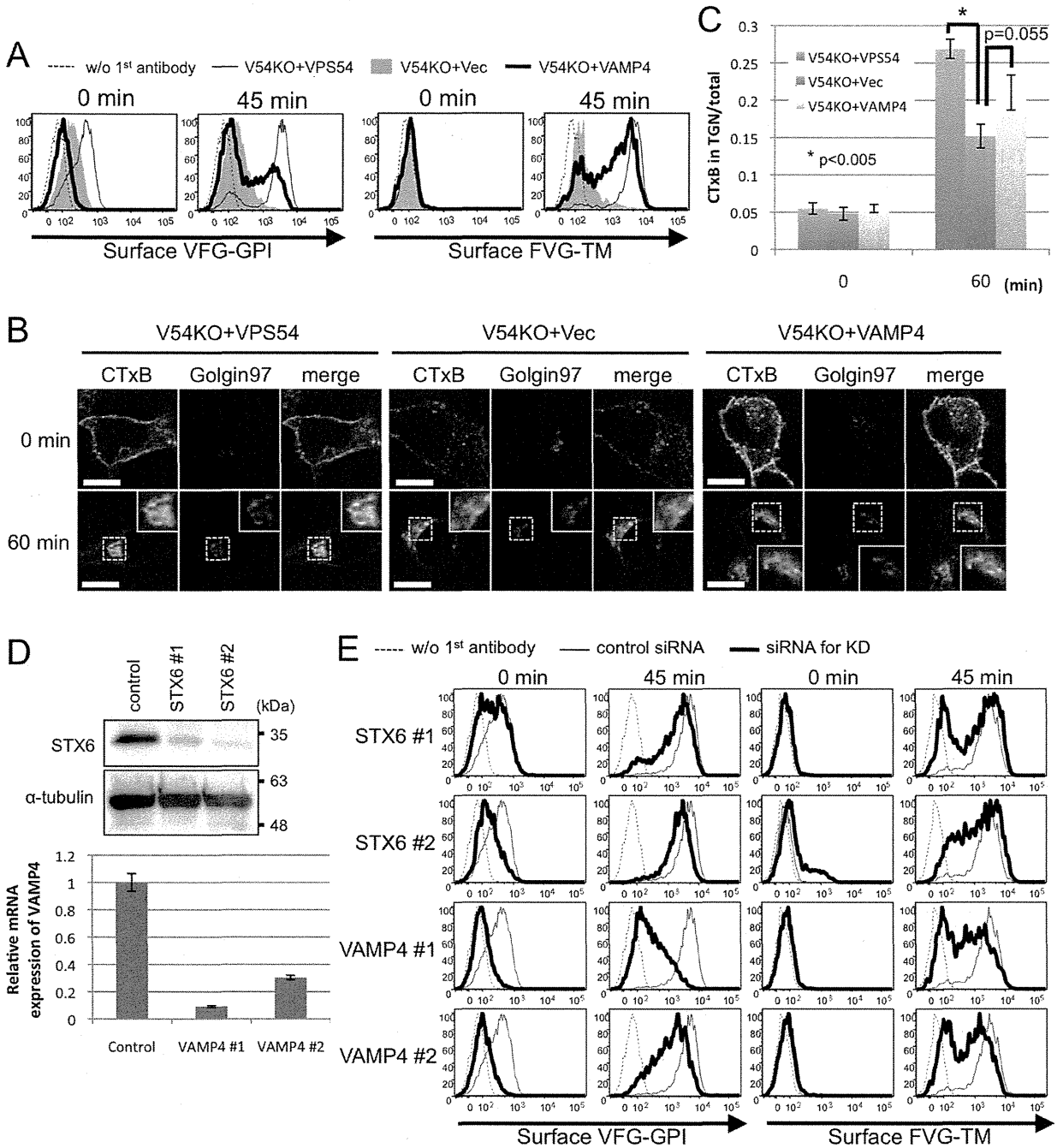

FIGURE 5: VAMP4-dependent retrograde transport is required for recycling of proteins critical for the post-Golgi anterograde transport. (A) Transport assay of VFG-GPI (left) and FVG-TM (right) in V54KO cells transiently transfected with the indicated genes. (B) Retrograde transport assay using CTxB. Cells incubated with Alexa Fluor 488–conjugated CTxB for 30 min on ice, followed by a chase at 37°C for 0 or 60 min, were analyzed by confocal microscopy after staining with anti-golgin97 antibody. Green, CTxB; red, golgin97 as a TGN marker. Scale bars, 10 μm. Similar results were obtained in two independent experiments. (C) CTxB in the TGN was quantified. Data are the means of 10 independent images. Error bars represent the SEM ($n = 10$). Similar results were obtained in two independent experiments. (D) Estimation of knockdown efficiency. HEK293FF6 was transfected with indicated siRNAs, and the expression of STX6 or VAMP4 was analyzed by Western blotting or qRT-PCR, respectively. For Western blotting, α-tubulin was used as a loading control. For qRT-PCR, HPRT1 was used as a control. Here #1 and #2 are siRNAs targeting different sites. (E) Effect of STX6 or VAMP4 knockdown on anterograde transport. Transport assay of VFG-GPI (left) or FVG-TM (right) in HEK293FF6 or HEK293TM10 cells, respectively, transfected with indicated siRNAs.

Unlike TMEM87A and TMEM87B, overexpression of GPR107 or GPR108, a member of LU7TM family closely related to GPR107, did not restore the delayed transport of either VFG-GPI or FVG-TM in V54KO cells (Figure 6B; geometric means of cell surface levels of VFG-GPI and FVG-TM in V54KO+GPR107 were 1.21 ± 0.38 and 0.98 ± 0.11 times, respectively, those in V54KO+Vec [$n = 2$], and

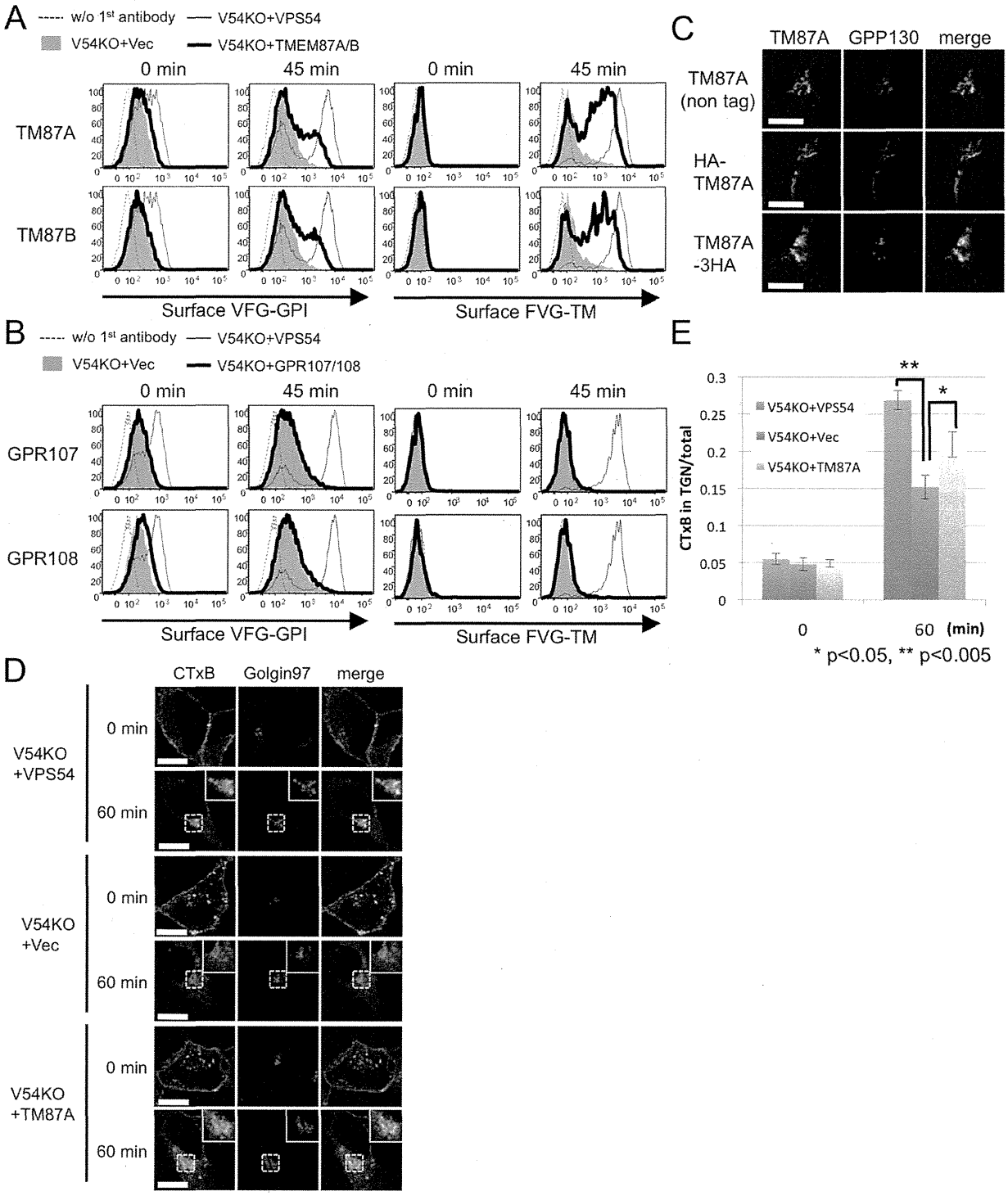

FIGURE 6: Potential role for TMEM87A and TMEM87B in endosome-to-TGN retrograde transport. (A) Overexpression of TMEM87A (TM87A) and TMEM87B (TM87B) partly rescues the delayed transport of proteins in V54KO cells. Transport assay of VFG-GPI (left) or FVG-TM (right) in V54KO cells transiently transfected with the indicated genes. (B) Overexpression of GPR107 and GPR108 does not rescue delayed transport in V54KO cells. Transport assay of VFG-GPI (left) or FVG-TM (right) in V54KO cells transfected with the indicated genes. (C) Subcellular localization of TMEM87A. Wild-type cells were transfected with nontagged or HA-tagged TMEM87A and double-stained with anti-TMEM87A (nontagged version) or anti-HA7 and anti-GPP130, a Golgi marker. Green, TMEM87A; red, GPP130 as a Golgi marker. Scale bars, 10 μm. (D) CTxB retrograde transport at 0 and 60 min. Green, CTxB; red, golgin97. Scale bars, 10 μm. Similar results were obtained in two independent experiments. (E) Quantitative data were obtained as described in the legend to Figure 5C. Data are the means of 10 independent images. Error bars represent SEM ($n = 10$). Similar results were obtained in two independent experiments.